LUDWIG MAXIMILIAN UNIVERSITY OF MUNICH
BACHELOR THESIS

Construction of an interference-filter-stabilized diode laser for experiments with ultracold strontium atoms

IVAN KOKHANOVSKYI
in collaboration with the Max-Planck-Institute for Quantum Optics
under supervision of Prof. Dr. Immanuel Bloch and Dr. Sebastian Blatt
Munich 2019

BACHELORARBEIT AN DER
LUDWIG-MAXIMILIANS-UNIVERSITÄT MÜNCHEN

Konstruktion eines interferenzfilterstabilisierten Diodenlasers für Experimente mit ultrakalten Strontiumatomen

vorgelegt von IVAN KOKHANOVSKYI
München den 25. Juli 2019

Abstract

In this Bachelor thesis we report on the construction of an interference-filter-stabilized external cavity diode laser at a wavelength of 689 nm for use in experiments with ultracold strontium atoms. This work contains a step-by-step explanation of the laser construction, including advice for installing each laser component. Furthermore, we describe control systems and wavelength selection mechanisms that enable stable single-mode operation of the laser. Optimization of the laser output power, its wavelength tuning and a determination of its linewidth are discussed. We also make suggestions for possible improvements in future iterations of the design.

Contents

List of Tables

List of Figures

Chapter 1

Introduction

The physical principle of light amplification by stimulated emission was predicted by Albert Einstein in 1916. In 1960 the first laser was constructed by C. H. Townes, N. G. Basov and A. M. Prokhorov [1, 2]. Now lasers are used in an enormous variety of devices operating in different research applications, both in physics and other sciences.

One of these research applications is laser cooling and trapping of neutral atoms [3]. Lasers used for this purpose have stringent requirements: they should be spectrally narrow compared to the width of the transition on which the atoms are cooled, have good thermal and mechanical stability, and be immune to acoustic noise as much as possible.

In this Bachelor thesis we describe the design, construction and characterization of a linear interference-filter-stabilized external cavity diode laser (ECDL) [4–6], with emission at 689 nm. The laser is intended to be used as part of an ultracold atom experiment based on strontium atoms. Therefore this particular wavelength was chosen so as to be able to address the $^1S_0 - ^3P_1$ transition in strontium [7]. The new interference-filter-stabilized ECDL would potentially replace the strontium lab's only 689 nm laser with Littrow configuration. I was tasked with construction and characterization of this laser. This Bachelor's thesis reports on its setup and investigations of its properties.

We give a brief overview of the thesis. The second Chapter begins with an explanation of laser physics and particularly focuses on semiconductor laser devices. This theoretical background explains the basic working principles of a semiconductor laser.

In the third Chapter we describe the mechanical construction of the laser and the optical alignment procedure required to enable single-mode operation. We explain step by step how the interference-filter-stabilized laser should be built, consider problems encountered with the setup, and propose possible solutions.

In the further Chapter we explore the optical elements needed for the optical setup. The schematic of self-designed optical setup is also presented.

The properties of the laser are described in the final Chapter. The laser provides output power of up to 40 mW at a maximum current of 140 mA. Additionally, we investigate how the operating temperature influences the spectral properties of the laser and the threshold current condition. The key to wavelength tuning of the laser is the aforementioned interference-filter. Therefore, we experimentally investigate its band-pass shape and the wavelength tunability range at various temperatures. Moreover, we describe the different tuning mechanisms of the laser, which allow us to achieve single mode operation at arbitrary wavelength within the tuning range. The full width at half maximum was also determined using an optical heterodyne method beat signal measurement.

Chapter 2

Fundamental Processes in a Laser

In the first Chapter, we describe the fundamental laws of laser action. We begin with the introduction of three processes in which energy conversion can occur. Then, we look at some properties of semiconductor diode lasers. Finally, the threshold condition is discussed.

2.1 Light-Matter Interaction

This Section begins with a short review of light-matter interaction processes. Let us consider a medium consisting of two-level quantum systems with a ground state with energy E_1, and an excited state with energy E_2. We take the number of atoms in the ground state to be N_1 and the number of atoms in the excited state to be N_2. The population ratio in the two states is given by the Boltzmann distribution [7]:

$$\frac{N_2}{N_1} = \frac{g_2}{g_1} \exp\left(\frac{E_1 - E_2}{k_B T}\right), \tag{2.1}$$

where g_1 and g_2 represent the degeneracy (the number of states with the same energy) of the ground and excited states, respectively, and k_B is the Boltzmann constant.

There are three processes relevant for understanding the operating principle of a laser: absorption, spontaneous emission and stimulated emission [8]. In the following we describe these processes in detail using Einstein's model (Fig. 2.1):

1. When resonant radiation is incident on the medium, an atom can be transferred from the ground to the excited state. This type of transition is called absorption and its rate is given by
$$\left(\frac{dN_1}{dt}\right)_{\text{ab}} = -B_{12} N_1 \rho(\nu), \tag{2.2}$$
where B_{12} is called Einstein's absorption coefficient, and $\rho(\nu)$ is the energy density which describes the amount of continuously emitted energy by atoms at temperature T and is given by Planck's law [7]:
$$\rho(\nu) = \frac{8\pi h \nu^3}{c^3} \frac{1}{e^{h\nu/k_B T} - 1}. \tag{2.3}$$

2. Spontaneous emission occurs, when an atom jumps down from the excited state to

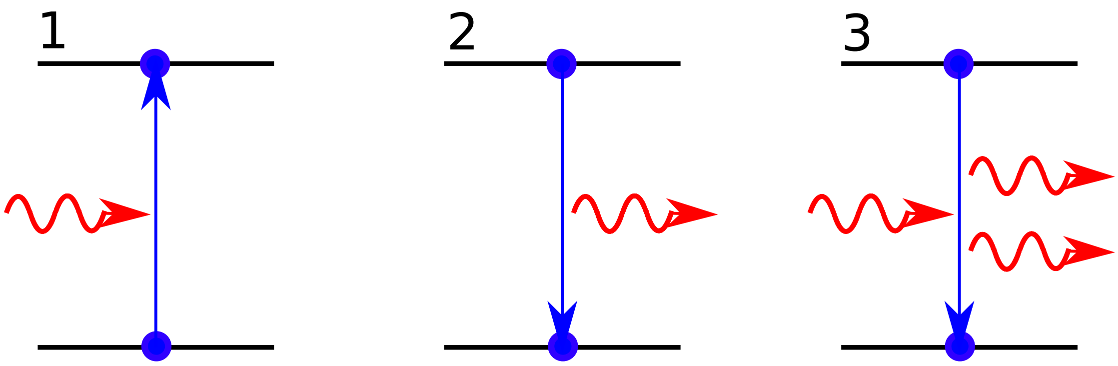

Fig. 2.1 Light-matter interaction processes in a two-level system: 1 - absorption, 2 - spontaneous emission, 3 - stimulated emission.

the ground state while emitting a photon of energy $E_2 - E_1$. The rate of decrease of the exited state population can be written as

$$\left(\frac{dN_2}{dt}\right)_{\text{sp}} = -A_{21}N_2, \tag{2.4}$$

where A_{21} is Einstein's coefficient describing the rate of spontaneous emission.

3. In the case of stimulated emission, atoms in the excited state are stimulated to make a transition to the ground state by an incident photon. This process leads to the emission of a second photon. The rate of this process is described by

$$\left(\frac{dN_2}{dt}\right)_{\text{st}} = -B_{21}N_2\rho(\nu), \tag{2.5}$$

where B_{21} is the Einstein's coefficient describing the rate of stimulated emission.

The sum of atom numbers in both states must be constant, which leads to

$$\frac{dN_1}{dt} = -\frac{dN_2}{dt},$$

and

$$A_{21}N_2 = (B_{12}N_1 - B_{21}N_2)\,\rho(\nu). \tag{2.6}$$

Applying Eq.(1.1-1.6) one can derive Einstein's relations

$$\boldsymbol{\frac{A_{21}}{B_{21}} = \frac{8\pi h\nu^3}{c^3}}, \tag{2.7}$$

$$\boldsymbol{g_1 B_{12} = g_2 B_{21}}. \tag{2.8}$$

2.2 Light Amplification

Let us consider now a light wave passing through an active medium. According to Eq.(2.2 - 2.5) this process causes stimulated emission and absorption in the active medium. If the rate of stimulated emission exceeds the rate of absorption, the wave will grow in irradiance (power per unit area). In a small path element dz, the change in irradiance is proportional to the difference between the rate of stimulated emission and absorption

$$dI(z) = [B_{21} N_2 \rho(\nu) E_{ph} g(\nu) - \alpha] \, I(z) dz, \tag{2.9}$$

were the spectral function $g(\nu)$ describes the frequency spectrum of the spontaneously emitted radiation, and α is an absorption coefficient. The irradiance can also be presented as a product of the energy density and the speed of light $I = \rho(\nu)c$ [8, 9]. From Eq.(2.6 - 2.8) we can rewrite this expression as

$$\frac{dI}{dz} = \left[(N_2 - \frac{g_2}{g_1} N_1) \frac{A_{21} c^2}{8\pi\nu^2} I(z) g(\nu) - \alpha \right] I(z), \tag{2.10}$$

and integrate over z to find

$$\boldsymbol{I = I_0 e^{(\gamma(\nu) - \alpha) z}}, \tag{2.11}$$

where $\gamma(\nu)$ is the gain coefficient. If $\gamma(\nu)$ is positive and larger then α, the irradiance grows exponentially with distance z.

2.3 Semiconductor Lasers

In this Section we give an overview of semiconductor lasers. First, we discuss the meaning of valence and conduction bands for semiconductor devices. Then we move on to the concept of a p-n junction. Finally, we describe the radiation mechanism of a semiconductor laser diode and discuss its basic properties.

2.3.1 Semiconductors

Electrons occupy quantized energy states [7]. For instance, in an atom with atomic number Z, electrons occupy the Z lowest energy states. Let us consider N atoms that form a solid. According to the Pauli principle, electrons with the same quantum numbers cannot occupy the same spin state. Due to the interaction between the atoms, bands are formed each containing $2N$ (the factor two because of the electron spin) energy states. At absolute zero temperature the last fully filled band is called the *valence band*. The *conduction band* is the first empty band in semiconductors. These bands are separated by an energy gap. The required energy to add an electron at absolute zero temperature is given by the Fermi energy E_f. For semiconductors E_f is located in the band gap. Therefore, the added electron appears in the conduction band. With an increase in temperature, the electrons can overcome E_g because of thermal excitations [10].

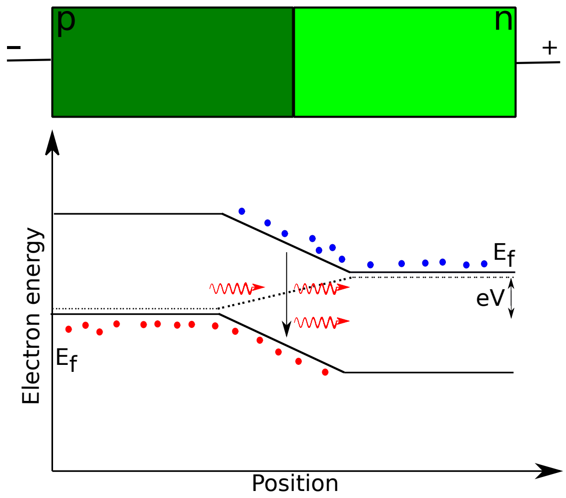

Fig. 2.2 A schematic of a forward-biased p-n junction. The horizontal axis represents the position, and the vertical axis the electron energy. The energy difference between the Fermi energies is given by eV, where V is the voltage due to the electrical field, and e is the electron charge.

The concentration of electrons and holes and the position of the Fermi energy can be changed by doping the material with electron donors (n-type) or electron acceptors (p-type). To understand the behavior of semiconductor devices, we begin by looking at the energy band diagrams of n- and p-type semiconductors. In n-type semiconductors the Fermi level is closer to the conduction band and in the p-type it is closer to the valence band. For further information about semiconductor devices Ref. [10] is recommended.

p-n junction Let us consider now what would happen when an n-doped and a p-doped region are put into a contact. Electrons from the n-region will diffuse into the p-region, where recombination with the abundant holes can take place. Similarly, holes from the p-region will diffuse into the n-region to recombine with the abundant electrons. The accumulated charge on both sides generates an electric field across the contact area. In this way, the Fermi levels line up and an energy barrier is produced. Applying a positive voltage to the p-region causes a misalignment of the Fermi levels in the p- and n-regions. The potential difference between the Fermi levels will increase. The injection of electrons into the conduction band and holes into the valence band by applying in external electric field will make the depletion region more narrow. This process generates spontaneous emission of photons by the electron-hole recombination mechanism, as sketched in Fig. 2.2.

2.3.2 Semiconductor Laser Diode

The laser diode is a semiconductor device a few hundreds of μm long and a few tens of μm thick (see Fig. 2.3). The function of a semiconductor laser diode is based on a

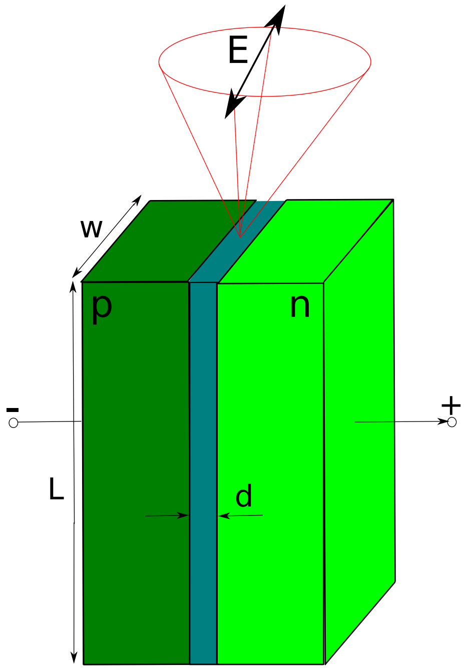

Fig. 2.3 A schematic of a semiconductor laser diode in a form of a forward-biased p-n junction. The active layer width is d, L is the cavity length,w is the laser diode width, and E represents a polarization.

forward-biased p-n junction constructed from a direct-bandgap semiconductor material (Fig. 2.3). In this case the positive terminal of the power supply is connected to the p-type side of the semiconductor laser diode and the negative one to the n-type. When a voltage is applied to the laser diode, the rate of electron-hole recombination processes increases. This process leads to an increase of the rate of stimulated emission. The light is generated by stimulated emission in a thin layer called the active region, where the electron-hole recombination takes place. The active region also has optical losses such as mirror losses or free-carrier absorption.

In the following Section we discuss some basic properties of semiconductor Fabry-Pérot diode lasers such as optical gain, threshold condition, and beam polarization.

2.3.3 Resonator

To understand the physics behind light propagation in a laser diode cavity, we take as our model Maxwell's concept of light as an electromagnetic wave. According to this model an oscillating electric field and an oscillating magnetic field are oriented perpendicular to each other having the same frequency. The orientation of the electric field vector $\boldsymbol{E}$ in the plane perpendicular to the direction of the propagation describes the polarization. If all the photons have the same polarization the wave is called linearly polarized. The linearly polarized light propagating along the z axis with amplitude E_0, wavenumber k,

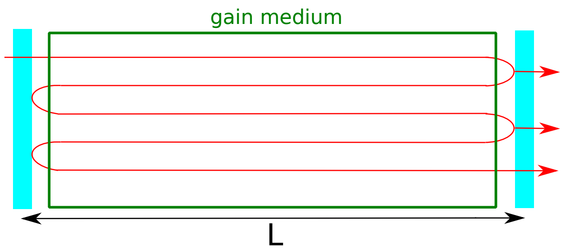

Fig. 2.4 The propagation of a plane wave between two mirrors in the gain medium. The length L describes the distance between mirrors.

frequency ω, and phase ϕ can be described as [8, 9]:

$$\boldsymbol{E}_z = \boldsymbol{E}_0 e^{(\omega t - ikz + \phi)}$$

In most lasers the active medium in which laser action happens is inside an optical resonator. Let us consider a plane wave propagating in a semiconductor laser cavity of length L (Fig. 2.4) consisting of two mirrors with transmission coefficients t_1, t_2 and reflection coefficients r_1,r_2, respectively. The field just after the left mirror is given by $t_1 E_0$. Traveling through the cavity, its phase grows until the second mirror is reached. A part of $r_2 t_1 E_0 e^{-ikL}$ will be reflected back into the cavity and a part $t_2 t_1 E_0 e^{-ikL}$ will be transmitted. The following process repeats and the final transmitted electrical field is given by a superposition

$$E_t = t_2 t_1 E_0 e^{-ikL} + r_1 r_2 t_1 E_0 e^{-3ikL} + (r_1 r_2)^2 t_2 t_1 E_0 e^{-5ikL} + \dots, \tag{2.12}$$

and can be calculated as a geometric series

$$E_t = E_0 \frac{t_1 t_2 e^{-ikL}}{1 - r_1 r_2 e^{-2ikL}} = \frac{E_0(1 - R^2)}{1 - R^2 e^{-i\delta}}, \tag{2.13}$$

where $R^2 = r_1 r_2$, $t_1 t_2 = 1 - R^2$ and $\delta = 2kL$ is the accumulated round-trip phase shift. The final transmission can be calculated as

$$T = \left(\frac{E_t}{E_0}\right)^2 = \frac{(1 - R)^2}{(1 - R)^2 + 4R \sin^2 \frac{\delta}{2}} = \frac{1}{1 + F \sin^2 \frac{\delta}{2}}, \tag{2.14}$$

where F is the finesse defined as

$$F = \frac{4R}{(1 - R)^2}. \tag{2.15}$$

The transmission maxima correspond to different oscillation modes, whose wavelength is given by

$$\lambda_m = \frac{2nL}{m}, \tag{2.16}$$

where n is the refractive index of the cavity medium, and m is the mode number.

Threshold condition Spontaneous emitted light propagating to the reflection mirror is amplified by stimulated emission in the gain medium. When the carrier density in the active layer of a laser diode is high enough to allow population inversion $\gamma(\nu) > \alpha$, stimulated emission becomes dominant over losses. This injection current value is known as the threshold current. By the threshold condition, the gain must be higher than the total round-trip loss. Mathematically, this requirement can be written as

$$R^2 e^{-2ikL} = 1. \tag{2.17}$$

The wavenumber k of a plane wave can be generally written as $k = \beta + i(\gamma - \alpha)$, where β is the propagation coefficient, γ is the gain of medium per unit length, which is provided by stimulated emissions, and α is the absorption coefficient [11]. Applying this form of k to the previous equation, one can rewrite it to

$$R^2 e^{2(\gamma-\alpha)L} e^{-2i\beta L} = 1. \tag{2.18}$$

We define the confinement factor Γ as $\Gamma = 1 - \frac{i\beta}{\gamma}$. Then, the threshold condition is given by

$$\boldsymbol{\Gamma\gamma = \alpha - \frac{\ln(R)}{L}}. \tag{2.19}$$

Laser diodes provide modes that are polarized parallel to junction (TE) and perpendicular to the junction (TM) (see Fig. 2.3). TE modes are strongly guided and have lower internal losses. A semiconductor laser diode usually have has TE polarization ratios of at least 100:1 in the case when the current is well above threshold [12].

Chapter 3

Laser Construction

In the previous Chapter, we discussed the basic properties of single-mode semiconductor lasers. The typical external cavity diode laser (ECDL) designs such as the Littrow and Littman-Metcalf configurations use diffraction gratings for wavelength tuning [13, 14].

In this Chapter, we are going to discuss an alternative ECDL, which operates with a narrow band-pass filter as the wavelength-selective part [4–6]. We begin with an introduction of the cavity design. Then, we move on to review the optics setup, electronic elements, and the mechanical construction of the interference-filter-stabilized ECDL. Furthermore, we consider problems encountered with the setup and propose possible solutions. Finally, we describe the optical alignment procedure for single-mode operation.

3.1 Design Overview

The basic setup of the external cavity diode laser is illustrated in Fig. 3.1. The light emitted by a laser diode (LD) with an antireflection-coated output facet is collimated by an aspheric lens in the collimator (CL). A partially reflecting mirror (output coupler OC with transmission of 0.70 and reflection of 0.3) provides the feedback into the diode. A high stability of the optical feedback is achieved by placing an aspheric lens with focal length $f = 18.40$ mm and numerical aperture $\mathrm{NA} = 0.15$ (a small rotation of the mirror will not cause the misalignment) in front of the output coupler (OC) at the focal length distance. The position of the OC can be tuned by a piezo-electric transducer (PZT) for the purpose of cavity length variation. A narrow-band high-transmission interference

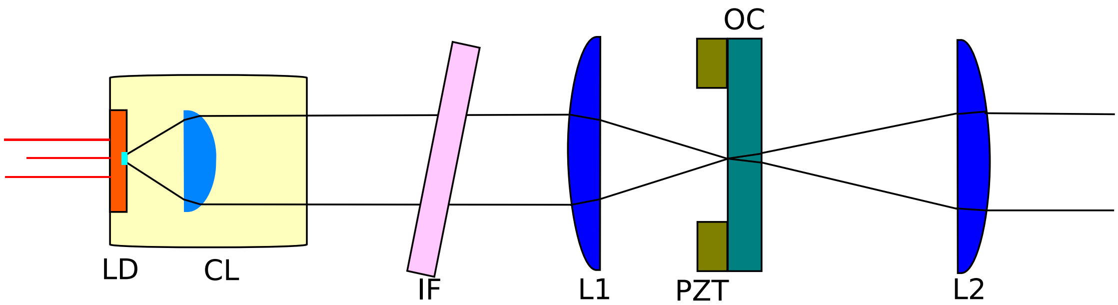

Fig. 3.1 External cavity diode laser design. LD - laser diode, CL - collimator, IF - interference filter, L1 - aspheric lens, PZT - piezo-electric transducer, OC - output coupler, L2 - output collimation lens.

filter (IF) is located between the LD and OC and provides wavelength tuning. A second lens (f = 18.40 mm, NA = 0.15) should collimate the output beam. In contrast to the Littrow laser design, reflection and wavelength tuning in our case are performed by two different elements (OC and IF) [15]. The laser diode, collimation tube and cavity optics are placed in an aluminum housing to isolate them from the laboratory environment.

3.2 Interference Filter

The key to the wavelength tuning of the cavity is an intra-cavity interference filter. Its wavelength selectivity is based on multiple reflections between two highly reflective facets within its dielectric coatings and behaves as a thin Fabry-Pérot étalon. A filter of this kind may be constructed by depositing two reflective coatings with a thin glass plate between them [16, 12]. To understand what happens when we tilt the filter, let us consider the characteristics of the Fabry-Pérot interferometer. As we discussed in Chapter 2, its transmittance is given by the equation:

$$T = \frac{1}{1 + F \sin^2 \frac{\delta}{2}}, \tag{3.1}$$

where F is the finesse and $\delta = \frac{2\pi}{\lambda} nd \cos\beta$ is the phase shift of the interferometer with the refractive index n, the thickness d and the angle of incidence β. Due to the angle of incidence, the optical length increases with a factor $\cos\beta$ (see Fig. 5.4). The interference filter has periodic transmission peaks at wavelengths given by

$$\lambda = \frac{2nd\cos\beta}{m} = \lambda_0 \cos\beta, \tag{3.2}$$

where λ_0 is the wavelength causing maximum transmission at a normal angle of incidence and m is an integer. Using Snell's law, we can rewrite the transmitted wavelength of the filter as (see Fig. 5.4):

$$\lambda = \lambda_0 \sqrt{1 - \sin^2\beta} = \lambda_0 \sqrt{1 - \frac{\sin^2\alpha}{n^2}}, \tag{3.3}$$

where α is the incidence angle outside of the filter. The wavelength tuning can be accomplished by tilting the filter with respect to the incident beam.

A derivation of these equations can be found in Ref. [17]. Further information about optical properties of coatings for interference filters can be found in Refs. [18, 19].

3.3 Electrical Control Parts

The operation of a laser diode requires a highly stable current controller as well as an active control of the laser diode temperature. Because of this, in addition to a well-engineered mechanical design and optical alignment we need to provide an electronic system to ensure precise tunability and stability of a laser system. To do this, we combine

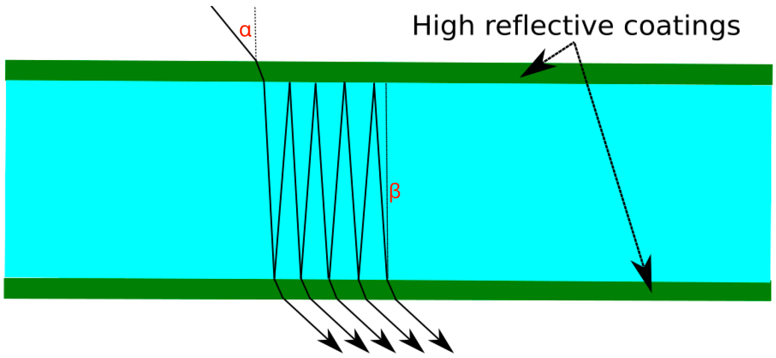

Fig. 3.2 Fabry-Pérot type interference filter with a sandwich design. The angle α is the incidence angle, β is a reflection angle in interferometer and n is the refractive index of glass.

two Peltier elements, a sensitive thermistor (Thorlabs TH10K) and an electronic control system (Toptica SYS DC 110) with a temperature control module (DTC 110) and current controller (DCC 110). To both protect the laser diode and to provide current modulation ports, an additional protection board is integrated into the housing. The circuit is based on Ref. [20] and its schematic is attached in Appendix A. We use a male 9-pin sub-D connector cable for the temperature controller and a female sub-D connector cable for the current controller. The board offers the following features:

1. A combination of four low-pass filters protects the laser diode from voltage spikes in the power supply.
2. Schottky diodes protect the laser diode if the wrong input voltage polarity is applied.
3. Test points for a four-point measurement to determine the current running through the laser diode. The foil resistor used here has a resistance of $R = 0.1\ \Omega$ and by measuring the voltage U, the current can be calculated from

$$I = \frac{U}{R} = 10\ \frac{\mathrm{V}}{\Omega}. \tag{3.4}$$

4. If a photodiode is integrated in the case of the laser diode, its signal can be amplified and can be read out from an SMA connector. The photodiode amplifier requires an external 15 V power supply.

3.3.1 Temperature Control System

In Fig. 3.3 we illustrate the three main components of the thermistor-controlled system, which regulate the temperature of the cavity. A 10 kΩ thermistor (Thorlabs TH10K) provides the electrical feedback to the Peltier device via a temperature controller (Toptica DTC 110). In the following Section we discuss how the thermistor can take and process

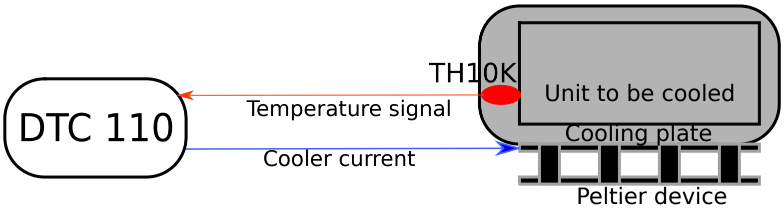

Fig. 3.3 Temperature control system consisting of Peltier device, TH10K thermistor, DTC 110 controller, cooling plate and the unit to be cooled.

the information about the temperature and what is the physical effect behind the Peltier device.

Thermistor Thermistors are thermally sensitive resistors and have, depending on the type, a negative (NTC), or a positive (PTC) resistance/temperature coefficient. NTCs offer mechanical, thermal and electrical stability, together with a high degree of sensitivity [21]. The relationship between temperature and resistance is not linear. A good approximation to explain the correlation between the temperature and the thermistor's resistance is provided by the Steinhart-Hart equation [21]:

$$\frac{1}{T} = A + B\ln(R/R_{25^\circ}) + C\ln^2(R/R_{25^\circ}) - D\ln^3(R/R_{25^\circ}), \tag{3.5}$$

where T is the temperature, R is the measured thermistor resistance, $R_{25^\circ\mathrm{C}}$ is the thermistor resistance at the temperature $25^\circ\mathrm{C}$, and A, B and C are constants. Further information about thermistors as thermometers and how the change in resistance can be converted into a feedback signal can be found in Ref. [21].

An epoxy-coated 10 kΩ thermistor with insulated leads is suitable for our purposes. In the temperature range from 0 °C to 50 °C the TH10K can be modelled with the data in Tab. 3.1 [22]:

$R_{25^\circ}(\mathrm{k}\Omega)$	$A(\mathrm{K}^{-1})$	$B(\mathrm{K}^{-1})$	$C(\mathrm{K}^{-1})$	$D(\mathrm{K}^{-1})$
10	3.354×10^{-3}	2.562×10^{-4}	2.141×10^{-6}	7.241×10^{-8}

Tab. 3.1 The data for thermistor (Thorlabs TH10K [22]): $R_{25^\circ\mathrm{C}}$ is the thermistor resistance at $25^\circ\mathrm{C}$, and A, B and C are constants.

Peltier element The second part of the temperature control system is a Peltier device. Its job is to heat or cool the cavity depending on the required temperature. We start with the discussion of the Seebeck effect and then move on to the commercial Peltier device and its application [23].

The Seebeck effect is a thermoelectric phenomenon that describes the generation of an electrical voltage due to a temperature difference between the ends of a thermoelectric

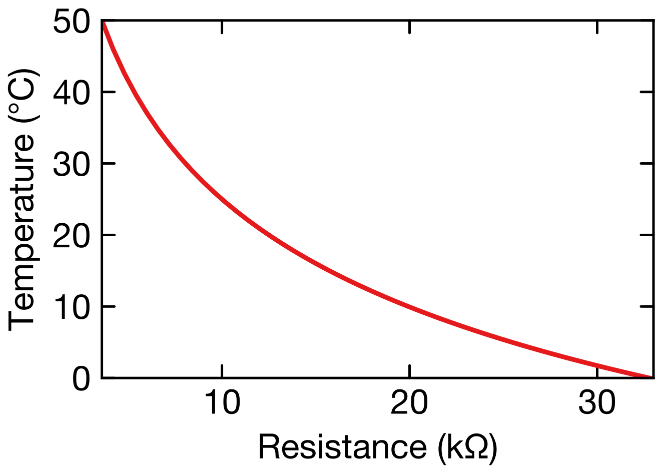

Fig. 3.4 Temperature versus resistance for TH10K.

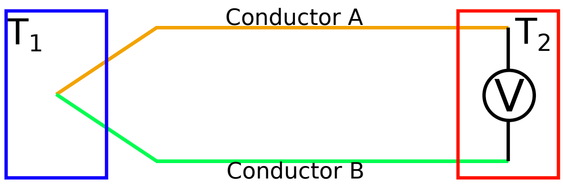

Fig. 3.5 Two conductors, A and B, in a temperature gradient $T_2 > T_1$. A net thermovoltage is measured with a voltmeter.

device. The Seebeck voltage depends on the material. For a small temperature difference ΔT, the relationship between the voltage difference ΔV and the temperature difference is approximately linear [24]

$$\Delta V = S \Delta T, \tag{3.6}$$

where S is the Seebeck coefficient. When two conductors A and B, having different Seebeck coefficients, are connected at two ends at the local temperature T_1 and the other two ends are at the local temperature T_2, the voltage difference between them can be measured (Fig. 3.5). This simple device is called a thermocouple. This effect occurs whenever electrical current flows through two dissimilar conductors. Depending on the direction of current flow, the system of two dissimilar conductors will either absorb or release heat. When $\Delta T = T_2 - T_1$ is not equal to zero, each conductor produces a thermovoltage. The magnitude of the measured voltage difference between the two conductors is

$$V_{AB} = V_A - V_B = S_A \Delta T - S_B \Delta T = S_{AB} \Delta T, \tag{3.7}$$

where $S_{AB} = S_A - S_B$ is the effective Seebeck coefficient of the conductor pair. Based on known temperatures, one can also predict the voltage V_{AB}.

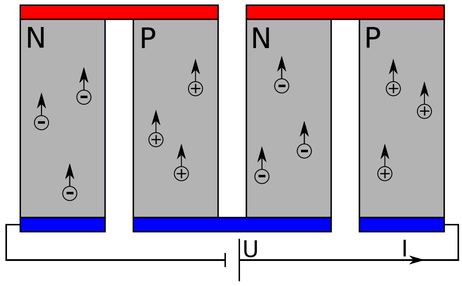

Fig. 3.6 A series of alternating n- and p-type semiconductor elements.

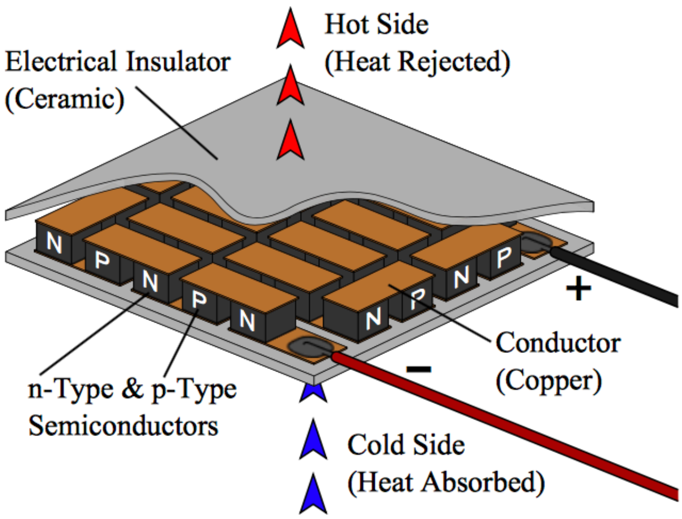

Fig. 3.7 The design of a commercial Peltier device. Adopted from Ref. [26].

The Peltier effect is the reverse phenomenon of the Seebeck effect. The Peltier element can be used to pump heat between two junctions, when a voltage is applied. Typically, a single Peltier element is not sufficient for technical solutions because of its small output power. To increase its output power, commercial Peltier devices consist of many n-type and p-type semiconductor elements, which are individually connected in series using hot and cold metallic junctions (Fig. 3.6). As a result of this, charge carriers flow freely in both directions and provide a heat flow in the same direction [25].

A complete Peltier device looks like a sandwich with two ceramic plates and a series of many p-n pairs (Fig. 3.7). As a consequence of this architecture, a large surface area can be achieved. The amount of heat pumped from one surface to the other depends on the applied current to the device.

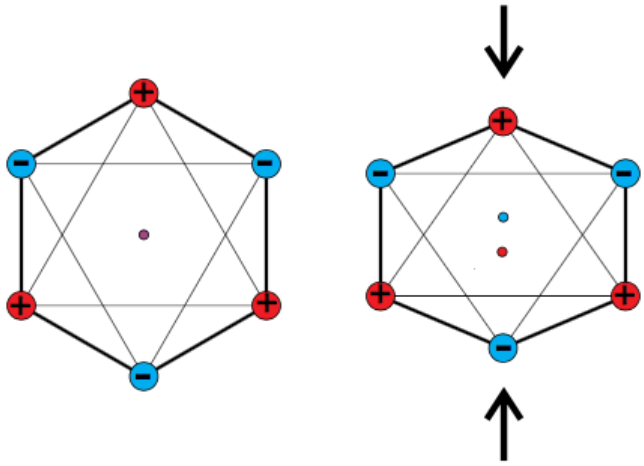

Fig. 3.8 Piezoelectric effect in a quartz crystal. The positively charged ions represent silicon and the negatively charged ions represent oxygen. Adopted from [27].

3.3.2 Piezoelectrically Tunable Resonator

Since the resonance frequencies of a cavity depend on its length, they can be changed by inserting a length-varying element like a piezoelectric actuator [27].

The phenomenon that the pressure applied to a piezoelectric material can produce an electric potential was first detected in 1880 by Jacques and Pierre Curie [28]. In such a material, the force along an atomic axis causes a charge balance change (Fig. 3.8). This imbalance results in the formation of an electric dipole and an electric field. Contrary, if an electric field is applied to a piezoelectric material, the crystal geometry will be deformed. This inverse piezo electric effect is used in piezoelectric actuators, whose length can be changed by applying a voltage.

For a physical description of the piezoelectric effect, a few basic relations have to be considered [27]. A dielectric material has the property that an applied electrical field E_j can produce a charge separation, which is explained by the polarization vector $P_i = \chi_{ij} E_j$, where χ_{ij} is the material's susceptibility. The total surface charge density is given by the dielectric displacement vector

$$D_i = E_i + P_i = (1 + \chi_{ij})E_i = \epsilon_{ij} E_j \qquad (i, j = 1, 2, 3). \tag{3.8}$$

Piezoelectric materials can be also polarized by applying mechanical pressure. Hook's law for linear elastic materials allows us to write the converse piezoelectric effect as

$$S_{ij} = d_{kij} E_k, \tag{3.9}$$

where S_{ij} is the strain tensor, and d_{ijk} is a third rank tensor containing the piezoelectric coefficients.

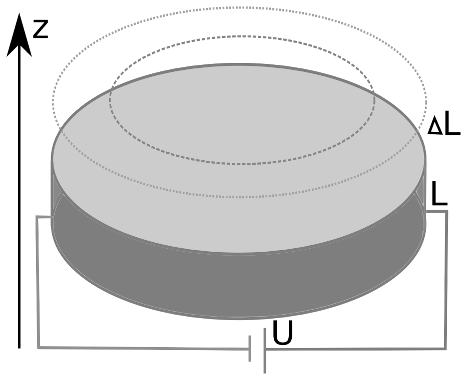

Fig. 3.9 Ring actuator length L changing with an applied voltage U.

There are many different piezoelectric materials which can be used for different applications. At the end of the 1940s, piezoelectric performance was discovered in lead zirconate titanate (PZT). At room temperature, its unit cell shows a dipole moment and has piezoelectric properties. Due to its high piezoelectric coefficient, PZT is the most used piezoelectric material [29].

The described materials can be used to build a ring piezoelectric actuator that operates according to the converse piezoelectric effect. The length change ΔL of a ring actuator along the direction of the electric field (Fig. 3.9) depends on the applied voltage U and the piezoelectric coefficient

$$\Delta L = S_z L = d_{zz} E_z L_0 = d_{zz} U, \tag{3.10}$$

where d_{zz} is the piezo-electric coefficient, U is the applied voltage, E_z is the electric field in the z-direction, S_z is a strain in the z-direction, and L is the ring width.

3.4 Mechanical Design of an ECDL

In this Section we report on the mechanical design of our ECDL, which was developed at MPQ (Max Planck Institute of Quantum Optics). The Figure 3.10 shows a 3-D schematic of the ECDL from two points of view (without cover). To avoid any construction problems, it is advised to complete the assembly of the ECDL step by step according to the following instructions.

Sonication After arriving from the machine shop, the mechanical parts are usually dirty and fatty with small particles sticking in the corners. Since the cavity will be located in a vacuum, every part must be cleaned very well. We clean the parts using an ultrasonic bath (Sonoswiss SW 90 H) with a frequency of 38 kHz [30]. In this bath the air bubbles grow and collapse, which can remove organic compounds from the surface of the materials and in this way clean them. The whole cleaning process can be completed according to Ref. [4]:

1. Put the parts in the bath and sonicate them at 40 $^\circ\mathrm{C}$ for 5-10 minutes.
2. After the sonication, flush every surface with deionized water and then with acetone and isopropanol.
3. To remove the chemical components, flush every part again with deionized water.
4. After cleaning, dry and store all the parts on a clean surface, e.g. aluminum foil.
5. To avoid thumb prints, after this, all parts should be touched only with gloves!

Construction In the next step make sure that all the parts are dry and ready to use. We begin the assembly with cavity adjustment. In the following text all numbers refer to Fig. 3.10. The collimator is screwed into the front side of the small aluminum housing (4). The interference filter is mounted and sits on a 4 mm of length small cylindrical pin, which provides a stable mount position and allows the rotation (5). In this way the incidence angle of the beam can be easily changed by hand. To achieve a precise adjustment use the screw on the mount top (5). The optical feedback elements are housed in the different enclosures (1). The lens between them is placed in the circular hole (10). To avoid friction when the lens rotates, use a viton O-ring on the lens and put a small amount of vacuum grease (OKS 110) around it before inserting. Directly under the cavity housing are two Peltier elements (13). To ensure optimal thermal conductivity, thermal paste should be applied at each Peltier element interface. The Peltier elements, thermistor and piezo are connected to the protection board (8). To plug and unplug the laser without opening the housing, the backplate with vacuum feedthroughs is constructed (12) (*because of the design mistake the back plate requires a small hole drilling for piezo connection!*). To protect the laser from mechanical vibrations, the cavity housing is placed in a vacuum chamber (2). The ECDL setup is isolated from the optical table by placing it on a breadboard.

Assembling: out-coupler to piezo In our cavity design, the PZT ring must be glued by $TorrSeal$ to the output coupler mirror to manipulate the cavity length (see Fig. 3.11). In the following Section we will describe how to do this on the best way. A good strategy for this process is also presented in Ref. [31]. Firstly, place the output coupler mirror on a few layers of optical paper and check that the partially reflecting side points up. Second, make sure that the upper side is very clean. Then place the piezo on the mirror in the correct orientation. To be sure that the glue can not expand to the inside of the piezo ring, put only four small drops of glue in the corners. Finally, gently place a weight on the top of the piezo to distribute the pressure uniformly on the actuator (*but do not damage the output coupler!*). Just after finishing the gluing, it is a good idea to check by eye that everything is parallel and in good condition.

Assembling: Thermistor Now we describe the assembly of this type of thermistor. For best accuracy of temperature control, the thermistor has to be glued close to the unit to

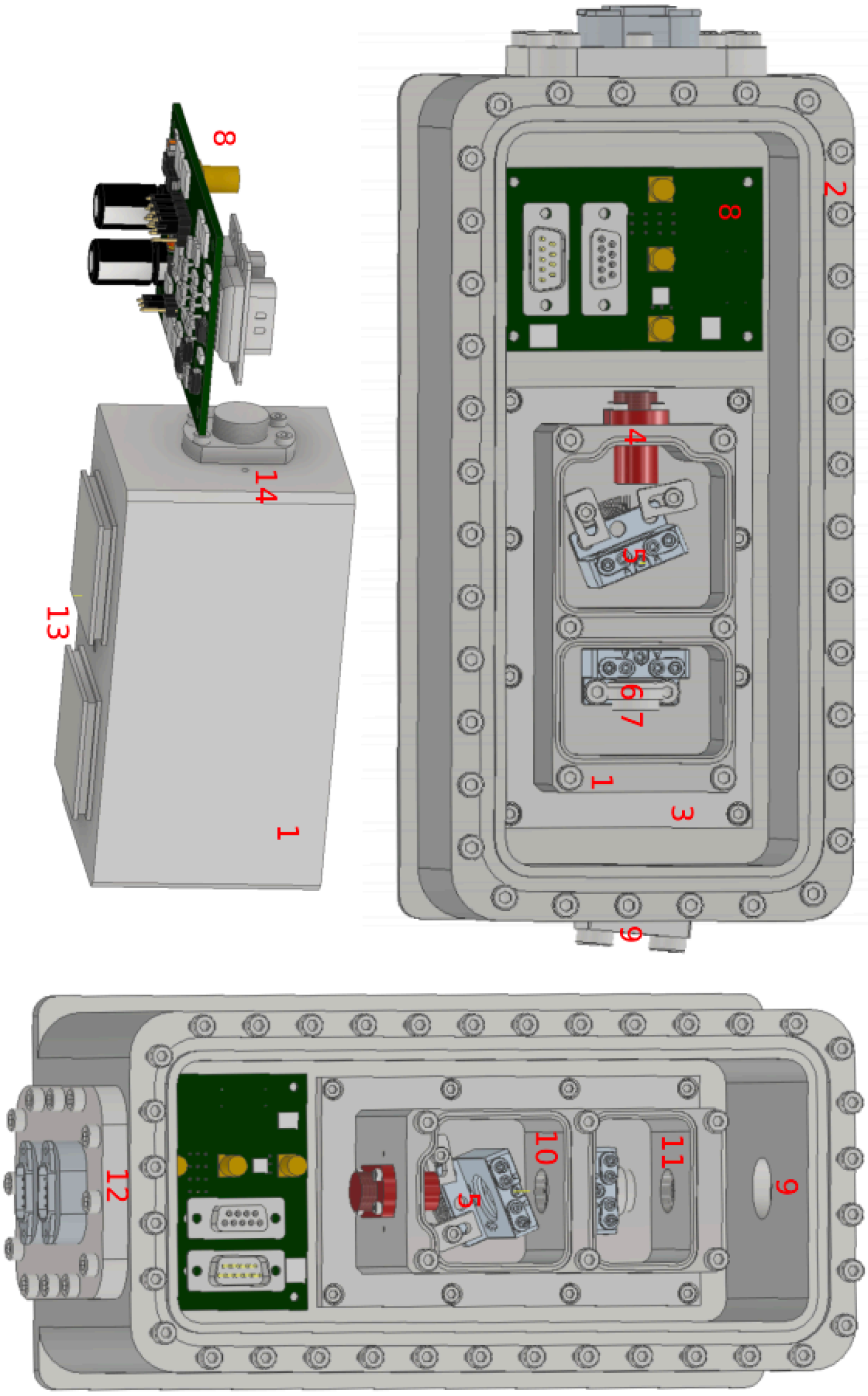

Fig. 3.10 A 3-D schematic of the mechanical design: (1) - cavity housing, (2) - vacuum chamber, (3) - thermoplate, (4) - collimation tube, (5) - interference filter, (6) - piezo, (7) - out-coupler, (8) - protection board, (9) - window, (10) - cat eye lens, (11) - collimation lens, (12) - backplate with vacuum feedthroughs , (13) - two Peltier elements, (14) - thermistor.

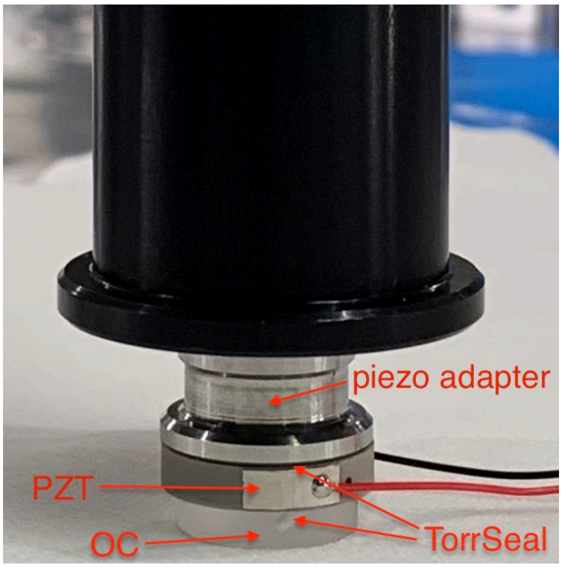

Fig. 3.11 The assembly of piezo to output coupler using $TorrSeal$ glue.

be cooled. In our case, it is located in the housing of the laser. We use EPO-TEK H74 thermally conductive epoxy with a mixing ratio of 100:3 by weight. The hole for the thermistor should be 6 mm in diameter (*additional drilling may be required*). After baking in the oven for one hour at 150 °C the glue should turn a dark red (Fig. 3.12).

3.5 Collimator

In the first chapter we described the structure of a laser diode. External-cavity semiconductor lasers are compact, easily pumped and have long lifetimes [15]. In our case we use a tunable Fabry-Pérot laser diode (*Eagleyard Photonics* EYP-RWE-0690-00703-1000-SOT02-0000) with parameters:

1. Cavity length L_D =1 mm.
2. Reflectivity at front facet $r_{ff} = 3^{-4}$.
3. Refractive index for λ = 689 nm at 20 °C - $n = 4.52$ [32, 33].
4. Recommended operating temperature range is from 15 °C to 20 °C.
5. At 20 °C the diode has a tuning range from 675 nm to 692 nm.
6. The absolute maximum current is $I_{max} = 140$ mA.

Due to the small size of its active layer, this type of laser diode has a wideangle radiation pattern. The emitted beam is divergent and requires associated optics, which

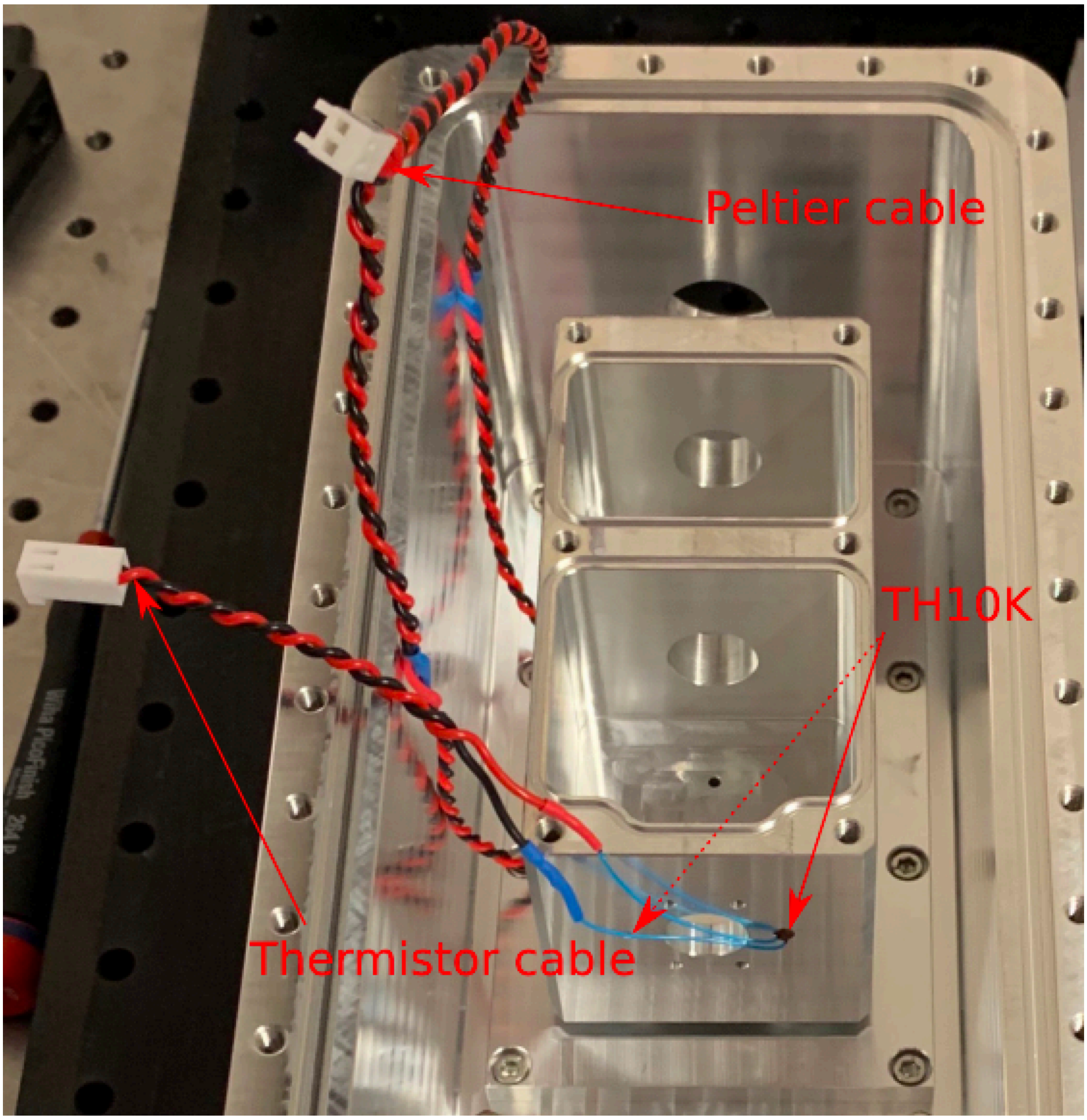

Fig. 3.12 The assembly of the thermistor into the cavity housing.

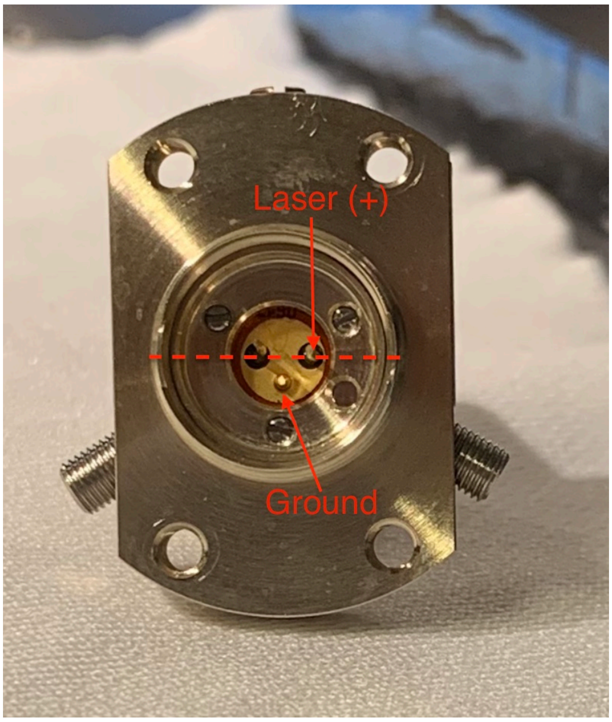

Fig. 3.13 Collimator from the back point of view.

provide efficient collection of the radiation [9]. This can be achieved with a collimator, which converts the divergent beam from a laser diode into a collimated beam. We use a collimator with an aspheric lens [34]. However, the beam profile is still elliptical as a result of astigmatism. For our cavity architecture we decided to use the collimator type (*Schäfter+Kirchhoff* 20C-A4.5-02), because it is compact and is simple to adjust.

In the following, we explain the collimator construction and adjustment procedure. It is important that one while working with laser diodes connects the workplace, equipment and oneself to Earth ground. Otherwise, the laser diode can be easily destroyed by static electricity discharge. First, one should check that there are no metal chips inside the collimator, which can generate short circuits. After inserting the laser diode into the collimator, one should try to center it as good as possible. For further information about mounting of a laser diode into this collimator refer to Ref. [34].

For the adjustment of the laser diode and collimation optics one should take into account the laser diode absolute maximum forward current of 140 mA. During the adjustment it is recommended to run the diode below its maximum condition. It is very important that the diode is well centered. This is achieved by adjusting three screws on the ring (see Fig. 3.13). To do precise adjustment it is advisable to remove the collimator from the laser and do the adjustment directly on the optical table. Concerning the elliptical beam shape of the laser diode emission, the semi-major axis of the ellipse should be aligned parallel to the table, such that the beam can be shaped later using a prism pair.

3.6 Aligning the Extended Cavity

Once the laser's mechanical setup is constructed and all electrical parts are ready to use, we can start with the alignment procedure. The Figure 3.14 shows a photo of the ECDL from the top. The laser beam should be reflected from the output coupler directly back into the semiconductor laser diode. Having successfully aligned and collimated the laser diode, one can proceed with the process of placing the remaining optics in the laser housing. The lens closest to the laser diode should be aligned first, since access to its mounting position is restricted by the housing of the laser. After assembly of the optics, the alignment of each component should be optimized. First, without the interference filter, the first lens should be aligned such that the beam is focused on the output coupler. To achieve lasing the laser diode and lens position must be perfect aligned. It is helpful to use a mirror-plate to reflect the laser beam vertically out of the housing and then to focus it in the far-field. Successive adjustment of the lens to maximize the cavity transmission may already lead to lasing. Secondly, the orientation of the output coupler should be optimized by changing its pitch and yaw via the adjustment screws on the mount. A combination of these two steps should result in optical feedback and lasing. In this case the laser diode starts lasing and the output power will increase dramatically. Finally, the last lens (L2) should be adjusted such that the beam is collimated in the far-field.

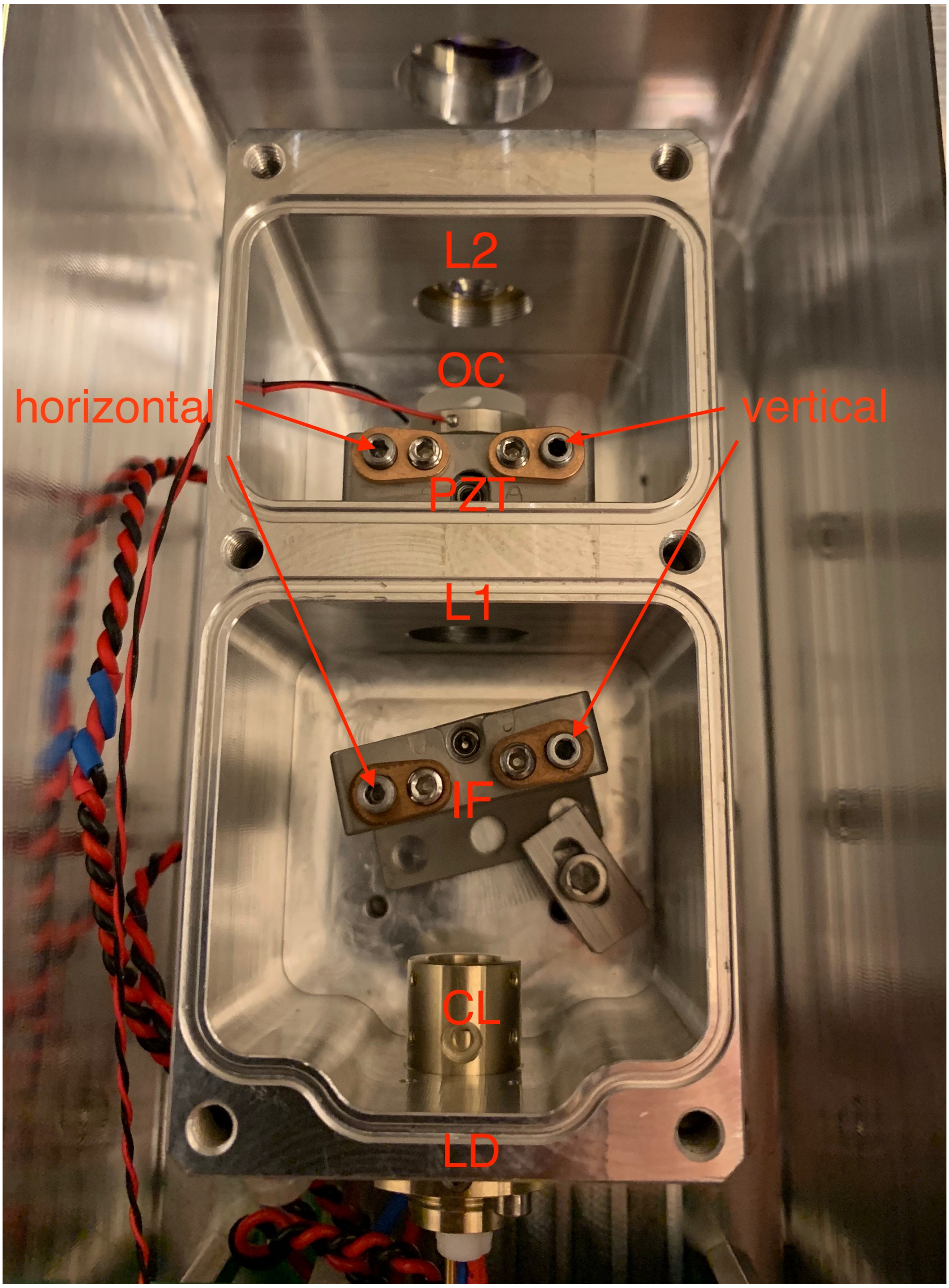

Fig. 3.14 The external cavity from the top view. LD - laser diode, CL - collimator, IF - interference filter, L1 - aspheric lens, PZT - piezo-electric transducer, OC - output coupler, L2 - output collimation lens.

Chapter 4

Optical Setup

The previous Chapter dealt with the laser construction procedure. In the following Chapter, we explore the optical setup outside of the laser cavity. As we discussed in Chapter 1, the output beam is elliptical and needs to be reshaped to match as closely as possible a TEM_{00} Hermite-Gaussian mode. The laser source must also be protected from back-reflections that can damage the laser diode or add noise. Furthermore, we want to check the laser's wavelength and simultaneously be able to measure the laser's properties.

This Chapter begins with a discussion on beam shaping. Then, we give an overview of optical devices, which are commonly used in similar optical setups. After this the self-built optical setup will be presented.

4.1 Anamorphic Prism Pair

The output beam shape can be investigated by a CCD and the software $RayCi$. The observed beam profile in the far-field, approximately 3 m from the laser, is shown in Fig. 4.1. According to a Gaussian fit provided by the software, the measured beam ellipticity is $\varepsilon = \frac{a}{b} = 3.58$ (see Fig. 4.1), where a and b represent the major and the minor axes of an ellipse, respectively.

We begin with the analysis of two general approaches of shaping the elliptical diode laser beam into a circular one. One way is to use cylindrical lenses, the other is to employ an anamorphic prism pair [11]. The advantages of cylindrical lenses (in the form of a telescope) over prisms are that the beam is not displaced from its original direction and that two cylindrical lenses can be adjusted to correct an astigmatism. Unfortunately, for large magnifications the telescope length becomes extremely long compared to that of a prism pair system. Moreover, the prisms are relatively easy to align. The most common prism configuration is the Brewster telescope as shown in Fig. 4.2. The magnification M of the prism pair is calculated in Ref. [11] and is given by:

$$M = \frac{D}{d} = \left(\frac{\cos A}{\cos B}\right)^2, \tag{4.1}$$

where A is the angle of incidence and B is the angle of refraction.

A mounted prism pair (Thorlabs PS881-B-N-SF11) provides the magnification of $M = 3.50$ with a beam displacement of $L = 6$ mm and is the best choice for the beam shape in our case [35]. This optical device should be mounted directly after the laser in such a way

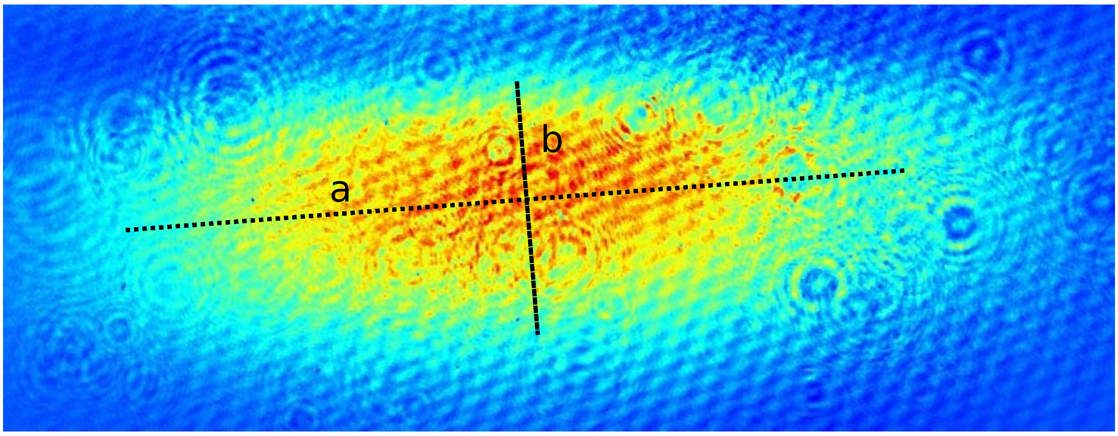

Fig. 4.1 Beam shape in the far-field taken by $RayCi$. Here, a is the major axis and b is the minor axis of an ellipse of the beam.

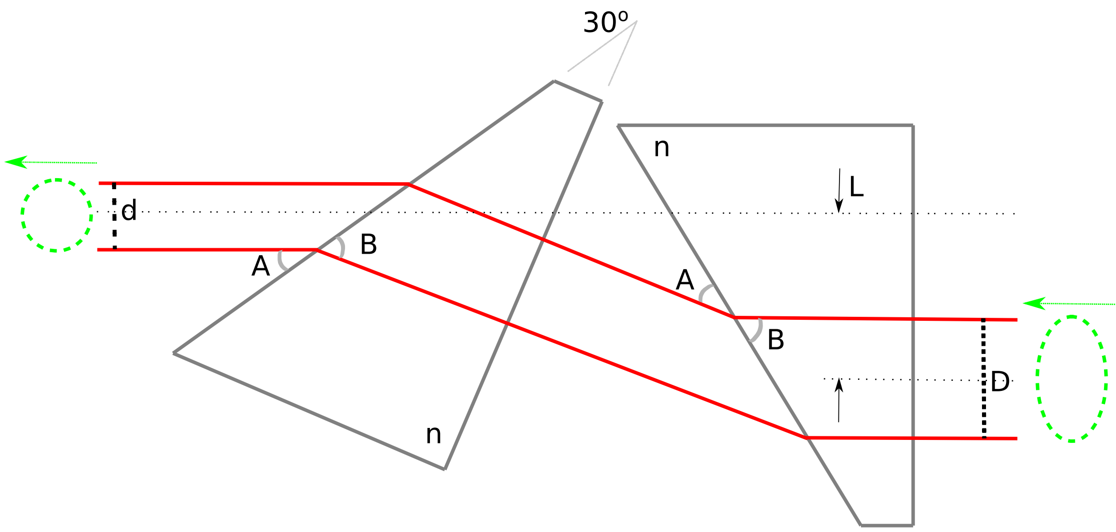

Fig. 4.2 Anamorphic prism pair configuration: n is the refractive index, A is the angle of incidence, B is the angle of refraction, L is the beam displacement, D is the input beam diameter and d is the output beam diameter.

that the beam's major axis will be reduced by a factor of 3.50 (see Fig. 4.2). In this way the beam can be reshaped in the far-field to achieve an ellipticity of $\varepsilon' = \varepsilon/M = 1.02$.

4.2 Optical Devices

In this Section we present the optical devices which compose the main part of our optical setup. Then, we move on to the structure of optical devices such as a Faraday isolator, a wave plate and polarizing beam splitter and discuss their applications.

Polarizer An electromagnetic wave can be made linearly polarized by using a polarizer. A polarizer can be constructed from a parallel grid of thin wires with a thickness small compared to the wavelength [8]. Due to the fact that only the electric field component perpendicular to the wires can be transmitted, such a device acts as a polarizer. According to Malus's law [8], when the beam passes through a perfect polarizer its intensity will be reduced by $\cos^2(\phi)$, where ϕ is the angle between the beam's initial polarization direction and the axis of the polarizer.

Isolator To avoid unwanted back-reflections into a laser source an optical isolator should be used. Even a very low level of optical back-reflection is sufficient to cause instabilities, power spikes or frequency shifts in single-frequency semiconductor lasers [9]. The solution is a Faraday isolator, which is consists of a Faraday rotator, an input and an output polarizer. To understand how the isolator should be aligned providing maximum forward transmission and reverse isolation, we describe the physical effects behind its function.

In 1845, Michael Faraday discovered that the polarization of light can be rotated in a magnetic field applied to a magnetooptic material [9]. This effect, known as the Faraday effect, occurs when a magnetic field is induced in the same direction as the path of the light. Different indices of refraction for the left and right circularly polarized light means that these rays propagate at different speeds through the medium. The Faraday rotator is a key component of an optical isolator. The amount of rotation is given by:

$$\theta = \nu B d, \tag{4.2}$$

where B is the magnetic field, d is the length of the magnetooptic material and ν is known as the Verdet constant, which depends on the material and varies on a small wavelength range as $\frac{1}{\lambda^2}$, where λ is the wavelength [36].

The first polarizer is adjusted to correlate with the polarization of the laser beam (see Fig. 4.4). The light traveling in Faraday rotator will become polarized at $45°$ in a clockwise direction, if the conditions for the Verdet constant are fulfilled. However, our laser beam deviates from isolator's central wavelength (see Fig. 4.3) and rotation is not an ideal $45°$. However, the isolator can be tuned maintaining full isolation and near-optimal transmission. Therefore, rotation at 689 nm is at $45°(\frac{670}{689})^2 = 43°$. The back reflected light must be rotated after the propagation in the Faraday device in the backward direction to

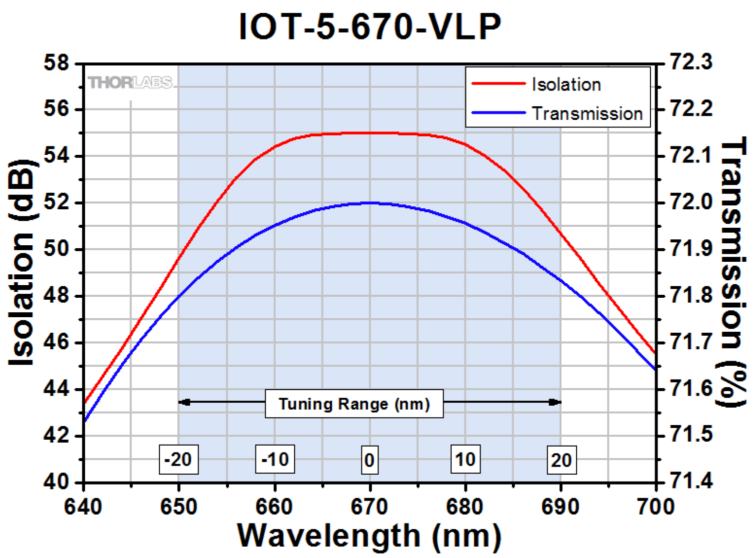

Fig. 4.3 Transmission and isolation profiles for IOT-5-670-VLP Faraday tandem isolator. The shaded region in this plot indicates the tuning range specified for this isolator. Adopted from [36].

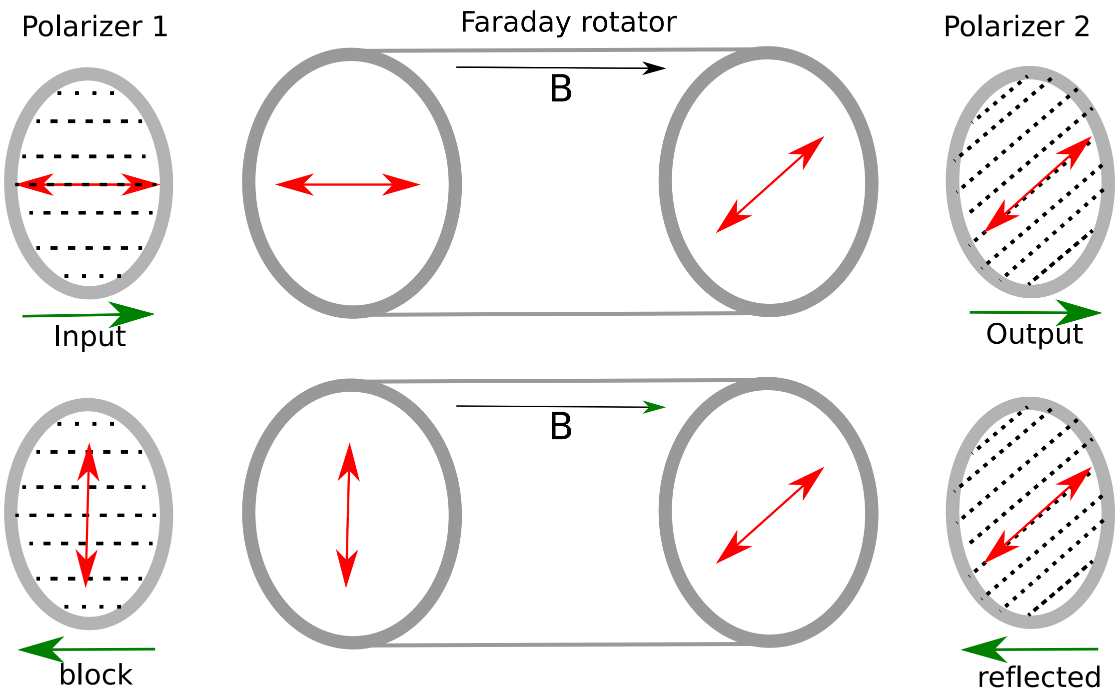

Fig. 4.4 A schematic view of an isolator with input and output polarizer and Faraday rotator. The figure above shows the forward light propagation and the figure below the backward light-propagation.

90° from the horizontal to ensure the full isolation. Because of this, the second polarizer must be rotated to $90^\circ - 43^\circ = 47^\circ$. In consonance with the Malus's Law the transmittance is additionally reduced by

$$1 - \frac{I}{I_0} = 1 - \cos^2(\phi) = 1 - \cos^2(47^\circ - 43^\circ) = 0.5\% \tag{4.3}$$

which is acceptable compared to the maximum transmission of 72%. In this way we can ensure the full isolation by losing only additionally 0.5% in transmission.

Wave plates Optical wave plates are constructed from materials which have different refractive indices for ordinary and extraordinary perpendicular axes. Let us consider two orthogonal components of the incident light on the plate that enter the wave plate in the same phase. Due to different speeds the component along the ordinary axis propagates faster than the one along the extraordinary axis. While the light passes through a wave plate, the phase shift δ grows and after a distance d it will be [8]:

$$\delta = \frac{2\pi d(n_e - n_o)}{\lambda}, \tag{4.4}$$

where n_e and n_o describe the different refractive indices along the extraordinary and ordinary axes, respectively. For the half-wave plate with $\delta = \pi$, the linearly polarized beam will remain linear but rotated by an angle 2θ, where θ is the angle between the polarization of incident light and the fast (ordinary) axis. In this way one can rotate the orientation of linearly polarized light.

Beam splitter Polarizing beam splitters are optical devices that can split a light beam into reflected s- and transmitted p-polarized beams. The commonly used splitters are constructed from two prisms and have a cube shape (Fig. 4.5). The hypotenuse surface of one prism is coated and joined with another prism with optical cement. To avoid the cement influencing polarization, the light should be transmitted into the coated prism, which is labeled with a reference mark on the surface.

Fiber coupling An optical fiber is a cylindrical dielectric waveguide constructed from a core and a cladding (Fig. 4.6). The core has a refractive index n_{cr} higher than a refractive of the cladding n_{cl}. This difference results in total internal reflection so that a beam can propagate along the fiber axis [9]. Applying Snell's law, the critical angle θ_{crit} for total internal reflection can be calculated from [8]

$$\cos\theta_{crit} = \frac{n_{cl}}{n_{cr}}. \tag{4.5}$$

The limited entering angle θ_a inside of which the beam will propagate within the core is determined by the equation

$$\sin\theta_a = n_{cr}\sin\theta_{crit}, \tag{4.6}$$

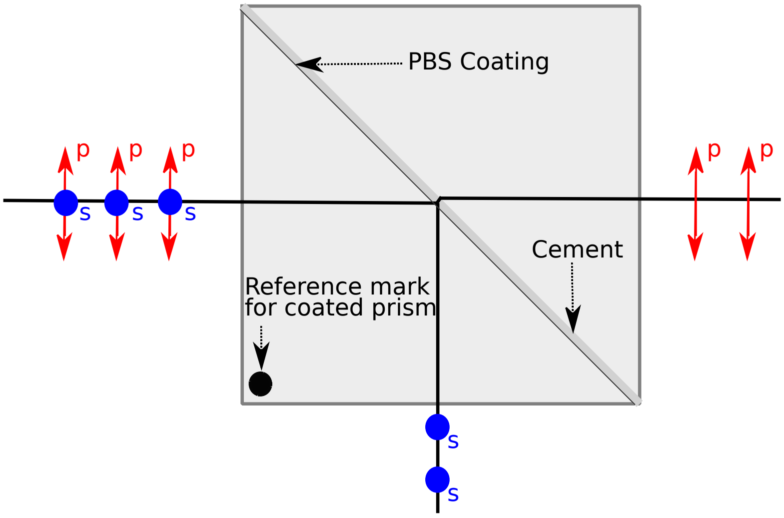

Fig. 4.5 Polarizing beam splitter cube. The beam enters the cube from left and will be divided into reflected s- and transmitted p-polarized beams.

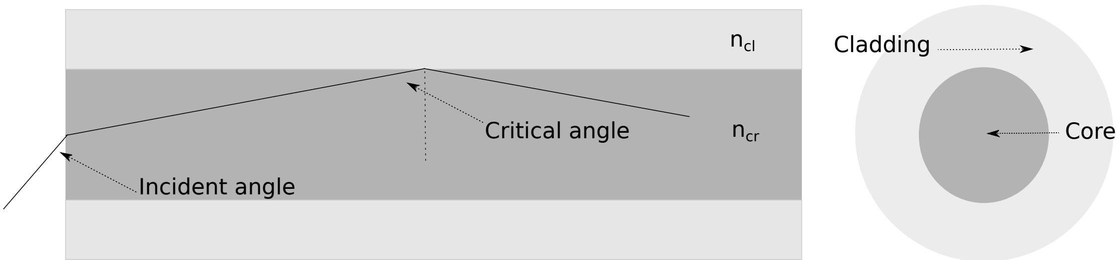

Fig. 4.6 Fiber guide from two points of view. Incident angle - θ_a, Critical angle - θ_{crit}, n_{cl} - a cladding reflective index, n_{cr} - a core reflective index.

and can be also expressed in terms of the numerical aperture

$$\mathrm{NA} = n_0 \sin\theta_a = n_0\sqrt{n_{cl}^2 - n_{cr}^2}. \tag{4.7}$$

The number of guided modes can be quantified by a number V, which is given by [9]

$$V = \frac{2\pi a}{\lambda}\mathrm{NA}, \tag{4.8}$$

where a is a core radius. If a/λ is small enough such that V is less then 2.4 [9], the fiber acts as a single-mode guide. This type of waveguide requires thin fibers with a core diameter less then a few wavelengths and a core refractive index should be slightly below the cladding refractive index [8].

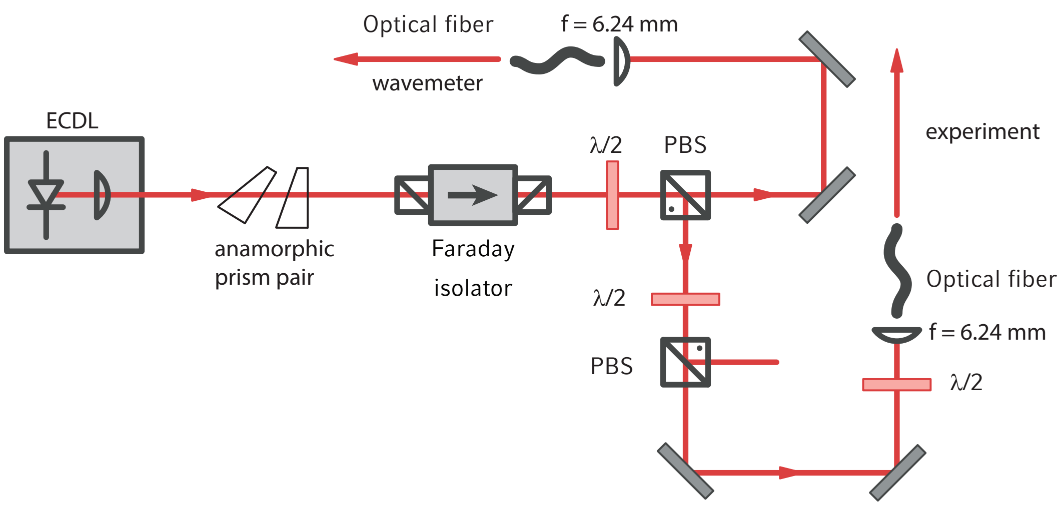

Fig. 4.7 A schematic of the optical setup on the bread board.

4.3 Optical Setup

Once all equipment for the setup is ready to use, one can proceed with the placing and aligning procedure. The schematic of the self-designed setup is illustrated in Fig. 4.7. This optical system offers the following features:

1. The elliptical output beam passes through the anamorphic prism pair and will be reshaped into a circular one.
2. The Faraday isolator is used to provide the isolation from back-reflections.
3. The first polarizing beam splitter (PBS) in combination with a half-wave plate splits a small amount of power to the wavemeter, while most of the power is reflected and sent to the experiment.
4. The second PBS with a half-wave plate in front is integrated to match the beam polarization with the slow axis of the optical fiber. Moreover, the s-polarized part can be used for future upgrades to the setup.

Chapter 5

Laser Properties

In this Chapter we explore the optical characteristics of our laser system such as output power, wavelength tunability, mode-hope free tuning range and linewidth. These properties are each presented in different sections. The most relevant are summarized in the conclusion.

5.1 Output Power

As discussed in the second Chapter, once the carrier density in the active layer is high enough for population inversion, stimulated emission dominates. The optical power emitted by stimulated emission in the laser diode cavity is proportional to the number of electron-hole recombinations and the photon energy. In this way the output power emitted from an ECDL can be written as

$$P = \eta(I - I_{th}), \tag{5.1}$$

where I_{th} is threshold injection current, and η is a slope coefficient, which includes a photon energy and an electron-hole recombination rate. The value of the threshold current depends on how well is the cavity aligned, i.e. how much optical feedback there is. By optimizing the output coupler orientation and lens positions one can minimize this parameter. This procedure leads to an increase in output power.

Threshold current optimization To proceed with the optimization procedure described in Ref. [31], one needs additional electrical equipment: a photodiode, a function generator and an oscilloscope. The function generator generates a triangle signal of 1 V peak-to-peak amplitude with a frequency of 50 Hz. The signal from the photodiode and the function generator are simultaneously displayed on an oscilloscope. While aligning the focusing lens and output coupler, one should monitor the signal on the oscilloscope and try to decrease the threshold current (see Fig. 5.1). By repeating this procedure a few times the threshold current can be minimized.

Once the threshold current is optimized, one can proceed with measuring the power output for single-mode operation at the desired wavelength of 689 nm. Figure 5.2 shows the ligth-current (LI) characteristics of the laser at various temperatures. Below the threshold current there are no visible changes in the output power. After further increasing the current a linear dependence of the output power was observed. From the

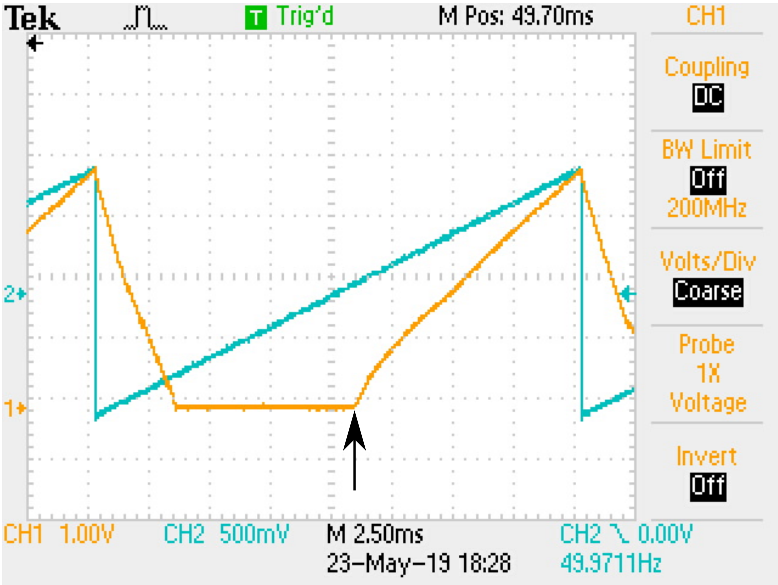

Fig. 5.1 Threshold current optimization using a function generator to modulate the current. The blue trace is the modulation signal, while the orange trace is the photodiode signal. The point, where the current reaches the threshold value is indicated with an arrow.

graph we can obtain I_{th} and η for different temperatures using a linear fit. Figure 5.3 shows the threshold current versus temperature. This dependence is described in the next section. We can see in Fig. 5.3 that the threshold current has a minimum at 20 °C and at the same time η is maximal. This means that to achieve maximum power output at 689 nm the laser should run at 20 °C.

5.2 Wavelength Selection

The principle of wavelength selection in an ECDL can be explained with the following model. The total gain function of an ECDL is given by a combination of the laser diode gain profile G_D, the transmission band profile of the interference filter T_{filter} and transmission functions of the cavity formed between the laser diode facet and the output coupler T_{cavity} [5]:

$$T_{total} = G_D T_{filter} T_{cavity} \tag{5.2}$$

The gain profile G_D can be assumed to be a broad Gaussian function having a full width at half maximum (FWHM) of approximately 15 nm [33]. The transmission profile of the filter as a function of wavelength was measured using a power meter and a second filter similar to the one in the laser (see Fig. 5.4). The transmission peak was fitted by a Lorentzian line shape giving a FWHM of 0.43 nm.

As discussed in Chapter 1, the cavity modes can be described as transmission modes

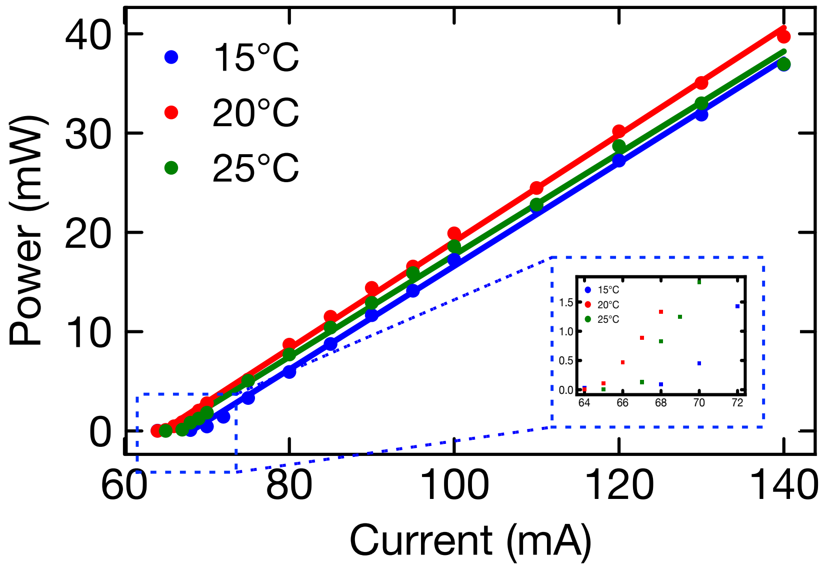

Fig. 5.2 Light-current characteristics of the laser at various temperatures.

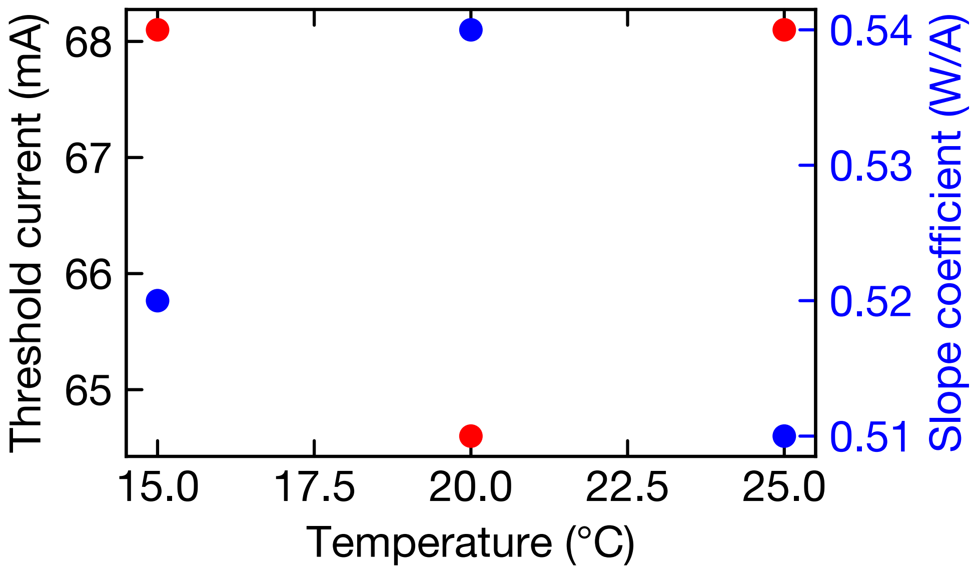

Fig. 5.3 The slope η (blue points) and threshold current I_{th} (red points) versus temperature.

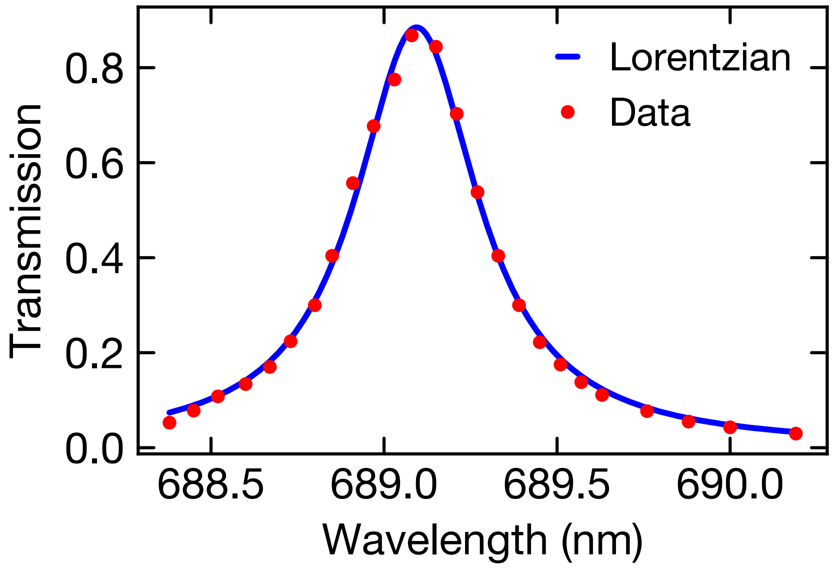

Fig. 5.4 Transmission profile of the band-pass of the filter optimized for transmission at 689 nm. The data is fitted with a Lorentzian function (blue curve) giving a FWHM = 0.43 nm.

of a cavity:

$$\lambda_m = \frac{2}{m}(L_{ext} + n_D L_D), \tag{5.3}$$

where $L_{ext} = 6$ cm is the external cavity length, $L_D = 1$ mm is the diode cavity length [33], $n_D = 4.52$ [33] is the laser diode refractive index and m is the mode number. In our case, the laser term $n_D L_D$ can be neglected, because $n_D L_D / L_{ext} < 4\%$. The mode spacing for $\lambda_m = 689$ nm is given by:

$$\Delta\lambda_m = \lambda_m - \lambda_{m-1} = \frac{\lambda_m^2}{2L_{ext}} = 0.004nm \tag{5.4}$$

There are other of parameters that can change the mode that has the largest peak, therefore, the operating wavelength. In the following section, we explore some of them.

Filter First, one can tilt the interference filter which leads to a shift of the band-pass position. The derivation of Eq.(3.3) gives:

$$\frac{d\lambda}{d\alpha} = -\frac{\lambda_0^2}{2\lambda n_{eff}^2}\sin(2\alpha), \tag{5.5}$$

For $\lambda_0 = 699$ nm, n_{eff}=1.7, and $\lambda = 689$ nm we get

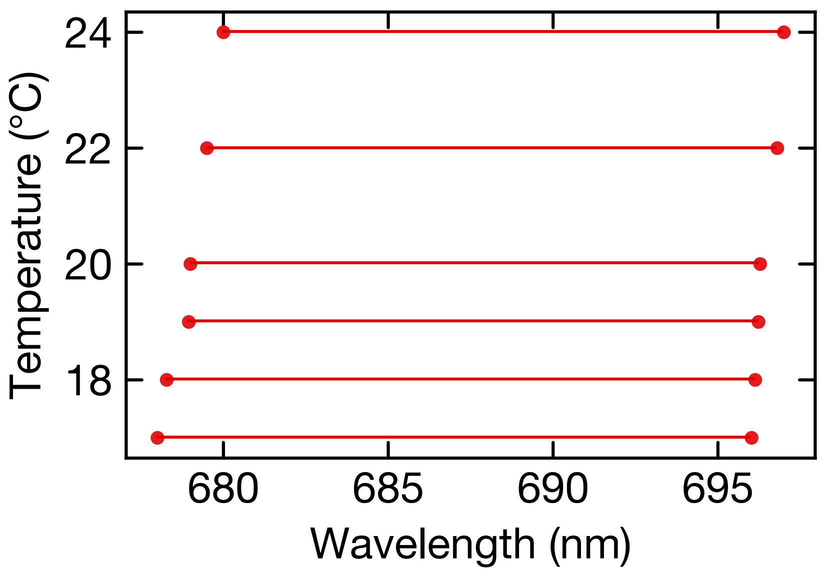

Fig. 5.5 Filter wavelength tuning range investigated for different operating temperatures.

$$\frac{d\lambda}{d\alpha} = 0.096 \left(\frac{\text{nm}}{\text{deg}}\right). \tag{5.6}$$

Moreover, the temperature influence on the wavelength tuning range via filter tilting was also investigated at various operating temperatures (see Fig. 5.5). We describe this dependence we move on the next Section.

Temperature The temperature dependence of the wavelength occurs because of several effects [4]. In the following, we discuss the most important of them. The optical path length varies because both the laser diode cavity length thermal expansion and the change of the refraction index of the semiconductor laser diode material. The correlation between the refractive index and energy gap can be described by different empirical relations. Some of them are presented and analyzed in Ref. [32]. To understand how the laser diode operating temperature influences the laser diode gain curve, we consider a linear model describing the dependence of the width of the band gap on the temperature:

$$E_g = E_0(1 - AT), \tag{5.7}$$

where $E_0 = 1.52$ eV is the width of band gap at T = 0 K and $A = 10^{-4}$ (K^{-1}) is a thermal coefficient of the semiconductor GaAs material [37]. We see that increasing the temperature causes contraction of the energy band gap and thus the wavelength changes

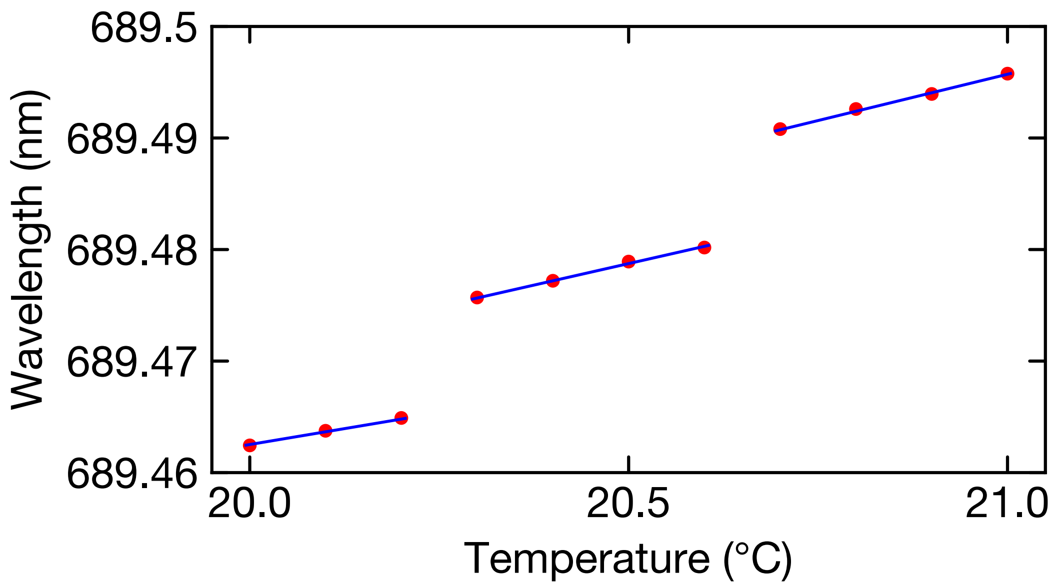

Fig. 5.6 Change of wavelength with temperature. Blue lines are linear fits to the data.

according to:

$$\left(\frac{d\lambda}{dT}\right)_{\text{gap}} = \frac{d}{dT}\left(\frac{hc}{E_g}\right) = -\frac{hc}{E_g^2}\frac{dE_g}{dT} = A\lambda\frac{E_0}{E_g} \tag{5.8}$$

The next significant effect is the thermal expansion of the metal housing. Due to cavity length variations the wavelength changes as:

$$\left(\frac{d\lambda}{dT}\right)_{\text{th}} = \frac{2}{m}\frac{dL}{dT} = \frac{\lambda}{L}\frac{dL}{dT} = k_{Al}\lambda, \tag{5.9}$$

where $k_{\text{Al}} = 2 \times 10^{-6}(K^{-1})$ is the thermal expansion coefficient of aluminum [4]. Due to both factors the change in wavelength is, therefore, given by:

$$\frac{d\lambda}{dT} = \left(k_{Al} + A\frac{E_0}{E_g}\right)\lambda = 0.075\ \frac{\text{nm}}{\text{K}}, \tag{5.10}$$

The graph in Fig. 5.6 shows the measured wavelength versus temperature for a current of $I = 140$ mA. By thermal tuning one can typically achieve a mode-hop-free tuning range on the order of $\Delta\lambda = 0.005$ nm. From Fig. 5.6 a slope of $\frac{d\lambda}{dT} = (0.037 \pm 0.005)\,\frac{\text{nm}}{\text{K}}$ can be obtained, what differs from our theoretical model. The coefficient A is probably lower for our semiconductor material.

5.3 Mode-Hop-Free Tuning Range

There are a lot of factors that determine the single mode laser frequency emitted by an ECDL: the gain profile of the laser diode, the internal resonator (laser diode cavity), the external resonator (optical system consisting the rare facet of laser diode and output coupler) and an interference filter. If the laser diode operation current or temperature change, the gain profiles shift asynchronously and with different rates. A simple way to check whether the laser is operating in a single mode, is to analyze the mode on the wavemeter. On the other hand, by scanning the piezo actuator, the length of the external cavity changes. In order to not cause mode hops the refractive index of the semiconductor material should also be simultaneously scanned, to compensate the optical length change of the cavity due to the piezo actuator. This is typically done by modulating the current with the same signal we use to modulate the piezo, albeit multiplied by a gain factor (typically much less then one). This feature is called *biasing* or *feed forward* and can be used to improve the the mode-hop-free tuning range of an ECDL. For the procedure of optimizing the mode-hop-free tuning range one needs a fast photodiode, an oscilloscope and a high voltage amplifier. We use the SC 110 controller from *Toptica*, which we described in Chapter 3. The adjustment procedure can be found in the Ref [38]. For our home-made laser we achieved a mode-hope free tuning range approximately of 2 GHz.

5.4 Linewidth

The light emitted by a laser ideally has a Lorentzian shape. However, mechanical vibrations of the cavity, temperature fluctuations, piezo voltage drive noise and current controller noise influences the line profile making it more broad [31]. The full width at half maximum (FWHM) of the spectral lineshape is called the linewidth. This parameter is one of the fundamental spectral properties of the laser. The purpose of this Section is to explain how was the linewidth of the home-build laser determined and compared with the linewidth of commercial lasers from *Moglabs* and *Toptica*.

The expression for the quantum-limited laser linewidth was presented in Ref. [39] and is known as the Schawlow-Townes unit:

$$\Delta\nu_{FWHM} = \frac{h\nu}{\pi P_{out}}(\Delta\nu)^2, \tag{5.11}$$

where P_{out} is the output power, ν is the frequency, and $\Delta\nu$ is the laser cavity linewidth. Typically, the linewidth predicted by Eq.(5.11) is about a two orders of magnitude smaller then observed for semiconductor lasers. This observation was justified by a few phenomena explained in Ref. [40]. To determine the experimental value of the linewidth and to compare it with commercial lasers, a series of optical heterodyne beat notes have been taken using a spectrum analyzer and a fast photodiode. A used setup is illustrated in the Fig. 5.7. To measure the linewidth it is necessary to overlap the beams on a photodiode and match the polarization of them. Assuming that the electric fields of both beams $\boldsymbol{E}_1$,

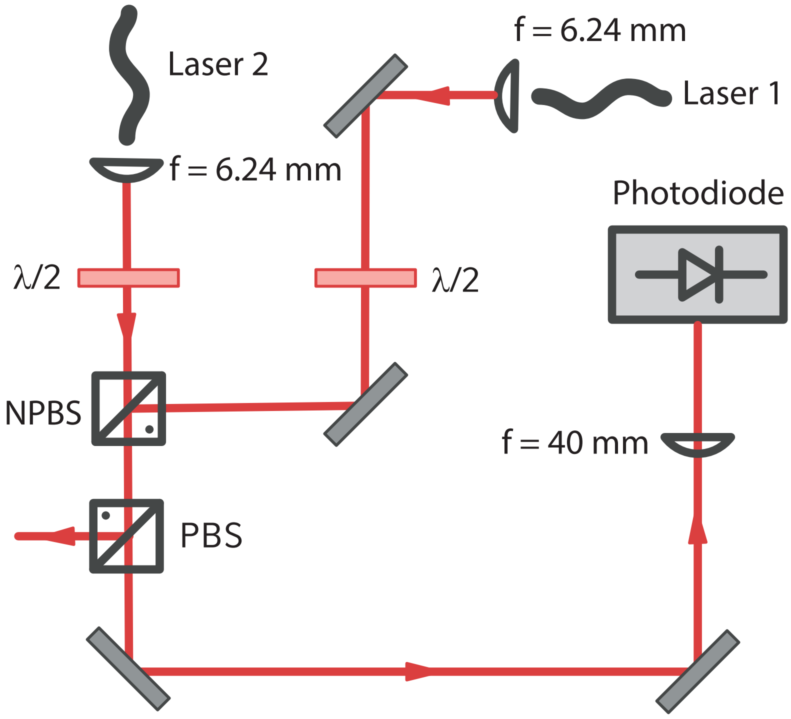

Fig. 5.7 A schematic setup of a beat signal measurement.

$\boldsymbol{E}_2$ are sinusoidal with frequencies ω_1 and ω_2, the intensity of the signal on the photodiode is proportional to the intensities of the incident light from the two laser beams and is given by

$$I \sim (E_1 \cos(\omega_1 t) + E_2 \cos(\omega_2 t))^2 = E_1^2 \cos^2(\omega_1 t) + E_2^2 \cos^2(\omega_2 t) + 2E_1 E_2 \cos(\omega_1 t) \cos(\omega_2 t)$$

using a simple trigonometrical identity and ignoring the constant part we can derive

$$I \sim 2E_1 E_2 \cos(\omega_1 t) \cos(\omega_2 t) = E_1 E_2 (cos((\omega_1 - \omega_2)t) + cos((\omega_1 + \omega_2)t) \tag{5.12}$$

The two laser frequencies must be close to each other so that the beat signal is within the bandwidth of fast photodiode. As we discussed in the previous Section, the wavelength can be coarsely tuned by varying the angle of the interference filter or changing the temperature. Fine adjustment can be achieved by tuning the length of the cavity with the piezo element [5]. Due to the higher frequency, the second term in Eq.(5.12) can not be detected even with a fast photodiode. The measurements of the beat note signals of two laser configurations are shown in Fig. 5.8 and Fig. 5.9. Since the *Toptica* laser is stabilized to a high-finesse cavity, its linewidth is significantly smaller than for the home-build laser. This means that the linewidth of the first beat gives us directly the linewidth of our laser

$$\Delta\nu_{home-made} = (271 \pm 30)\text{kHz}.$$

The *Moglabs* laser was not stabilized and the beat note frequency moved around more strongly than with *Toptica*. To avoid broadening of the line due to this effect several single measurements of 1 ms have been taken. Due to the technical frequency noise around the peak, the beat signal is well fitted with a Gaussian function. That is a convolution of the widths of the two lasers in question and is given by the following expression [5]:

$$\Delta\nu_{beat}^2 = \Delta\nu_{home-made}^2 + \Delta\nu_{Moglabs}^2. \tag{5.13}$$

Using this expression we find the linewidth of the *Moglabs* laser to be

$$\Delta\nu_{Moglabs} = (806 \pm 70)\text{kHz}.$$

This means that the linewidth properties of our laser is comparable to the commercial one.

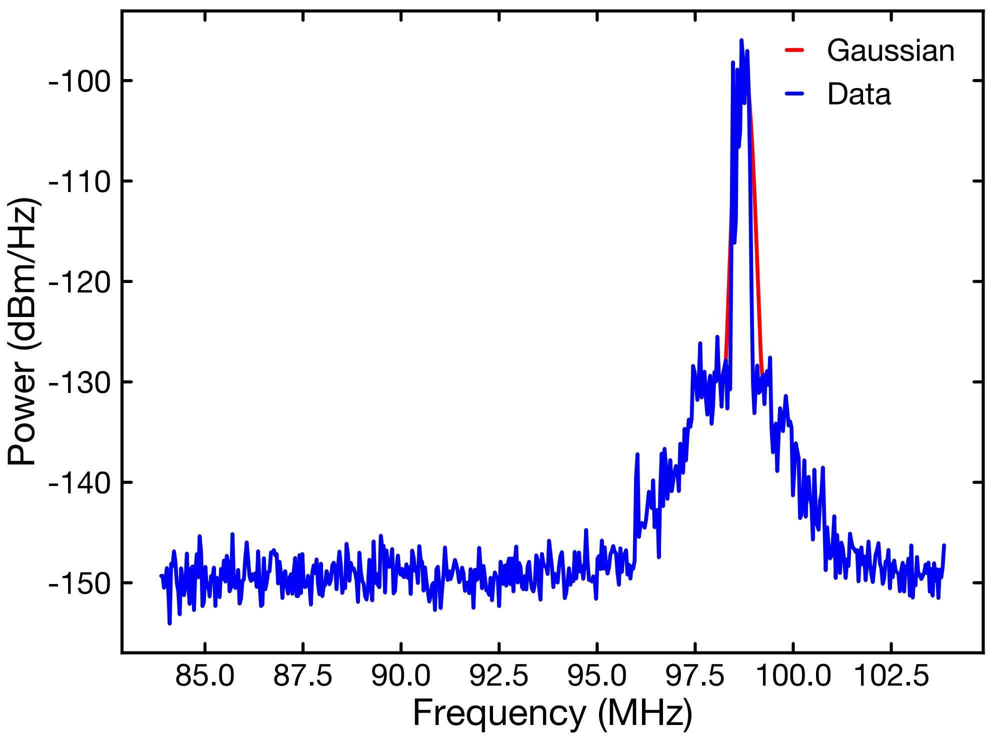

Fig. 5.8 A beat note signal of home-made laser and *Toptica*: $\mathrm{RBW} = 30\,\mathrm{kHz}$, sweep time 1 s, $\mathrm{FWHM} = 271\,\mathrm{kHz}$.

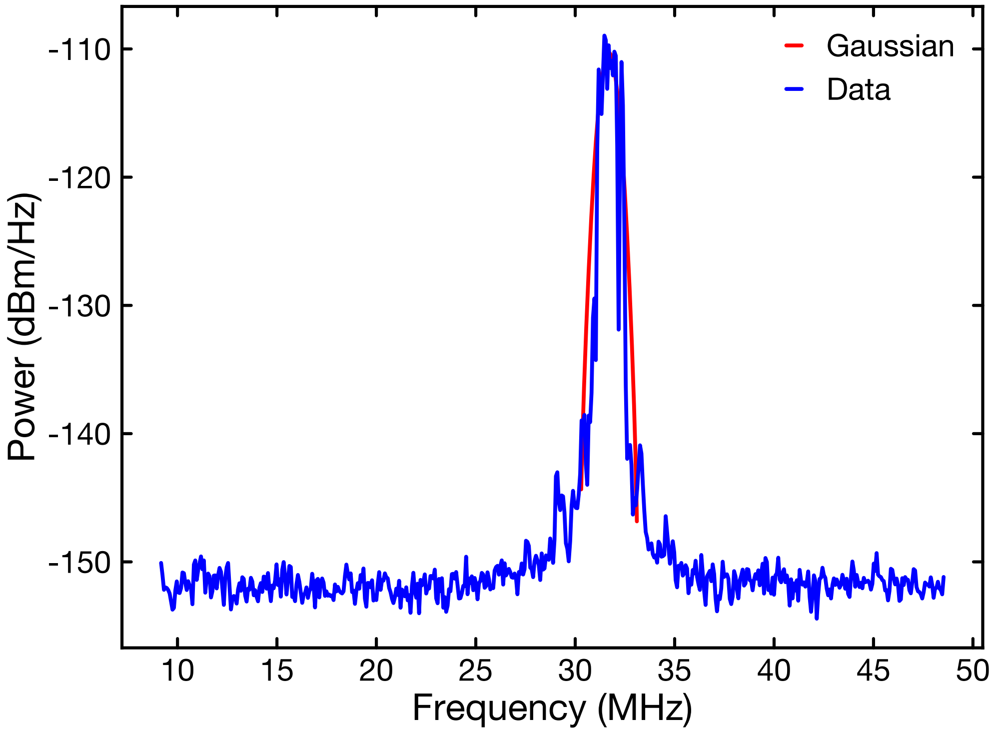

Fig. 5.9 A beat note signal of home-made laser and *Moglabs*: $\mathrm{RBW} = 300\ \mathrm{kHz}$, sweep time 1 ms, $\mathrm{FWHM} = 850\ \mathrm{kHz}$.

Chapter 6

Conclusion

To conclude, we described the design and construction procedure of an linear interference-filter-stabilized external cavity diode laser. Furthermore, we characterized the laser properties and discussed the possible improvements of the design.

By optimizing the threshold current, we found out that the home-made linear laser can provide a maximum output power of up to 40 mW at a maximum current of 140 mA. The lowest threshold current achieved was 64 mA observed at 20 $^{\circ}\mathrm{C}$. Single mode operation is provided by an extremely narrow interference filter with a FWHM of 0.43 nm. The wavelength tuning range achieved was from 678 nm to 697 nm at 20 $^{\circ}\mathrm{C}$. Moreover, the angular displacement sensitivity is equal to 0.096 (nm/deg) making the laser easy to align compared to traditional designs. The next advantage is that, in contrast to the Littrow laser design, reflection and wavelength tuning in our case are performed by two different elements (output coupler and interference filter, respectively) compared to a single element in the Littrow design (grating). An important advantage of the linear design is the cat's eye reflection geometry between the focusing lens and output coupler. This system is self-aligning and thus mechanically stable and robust. The linewidth (full width at half maximum) was found to be (257 ± 30) kHz by observing an optical heterodyne beat signal. This value is comparable with the linewidth of a commercial laser we also tested (*Moglabs*). We found that using only standard optical components, the optical setup of our ECDL is simple to build and align, yet robust and stable in use.

There are a number of features of the linear ECDL that can be improved. The long cavity length incorporated in our design results in a mode spacing of approximately 2 GHz. Because of this there is an increased tendency for the laser to mode hop, especially when scanning with the piezo actuator. In future iterations of the design the cavity length could be reduced. This will, however, broaden the linewidth, but this effect will most likely not be noticeable because, as we discussed, the observed linewidth is orders of magnitude above the Schawlow–Townes linewidth and can mainly be attributed to current and acoustical noise. The beam shaping could also be improved. As we discussed in the Chapter 3, the advantages of cylindrical lenses (in the form of a telescope) over prisms are that the beam is not displaced and that a cylindrical telescope can be adjusted to also correct for astigmatism. For longer beam paths the astigmatism could be a problem and one may need to replace the prisms.

With sufficient output power, wavelength tunability, narrow linewidth, combined with a simple and stable construction, the constructed laser is well suited for use in an ultracold atom experiment with strontium atoms.

References

[1] Siegman, A. E. *Lasers*. University Science Books, 1986. ISBN: 0935702113.

[2] Milonni, P. W. and J. H. Eberly. *Laser Physics*. 2rd edition. Wiley, 2010. ISBN: 978-0470387719.

[3] Metcalf, H. J. and P. van der Straten. *Laser Cooling and Trapping*. Springer, 1999. ISBN: 978-0-387-98728-6.

[4] Saliba, S. D., M. Junker, L. D. Turner, and R. E. Scholten. *Mode stability of external cavity diode lasers*, Applied Optics **48**., 6692 (2009). DOI: 10.1364/AO.48.006692.

[5] Gilowski, M., C. Schubert, M. Zaiser, W. Herr, T. Wuebbena, T. Wendrich, T. Mueller, E. Rasel, and W. Ertmer. *Narrow bandwidth interference filter-stabilized diode laser systems for the manipulation of neutral atoms*, Optics Communications **280**, 443 (2017). DOI: 10.1016/j.optcom.2007.08.043.

[6] Thompson, D. J. and R. E. Scholten. *Narrow linewidth tunable external cavity diode laser using wide bandwidth filter*, Review of Scientific Instruments **83**., 023107 (2012). DOI: 10.1063/1.3687441.

[7] Bransden, B. H. and C. J. Joachain. *Physics of Atoms and Molecules*. 2nd edition. Prentice Hall, 2003. ISBN: 978-0-582-35692-4.

[8] Smith, F. G. and T. A. King. *Optics and Photonics*. John Wiley and Sons, 2000, p. 439. ISBN: 0471489247.

[9] Saleh, B. E. A. and M. C. Teich. *Fundamentals of Photonics*. 2nd edition. John Wiley and Sons, 2007. ISBN: 978-0471358329.

[10] Shur, M. *Physics of semiconductor devices*. Pearson, 1990, p. 712. ISBN: I0-13-666496-2.

[11] Cunyun, Y. and T. K. Wei. *Tunable External Cavity Diode Lasers*. World Scientific Publishing, 2004. ISBN: 981-256-088-2.

[12] Duarte, F. J. *Tunable lasers handbook*. Optics and Photonics, 1995, p. 349. ISBN: 0-12-222695-X.

[13] Homeier, L. “Setup and characterization of a Littrow laser for 689 nm”. LMU Munich. Bachelor Thesis. 2016. URL: http://ultracold.sr/publications/thesis_lukas_homeier.pdf.

[14] Hong, W. and O. J. Painter. “Design and Characterization of a Littrow Configuration External Cavity Diode Laser”. Caltech, 2005.

[15] Baillard, X., A. Gauguet, S. Bize, P. Lemonde, P. Laurent, and A. C. and P. Rosenbusch. *Interference-filter-stabilized external-cavity diode lasers*, Optics Communications **266**, 609 (2006). DOI: 10.1016/j.optcom.2006.05.011.

[16] Born, M. and E. Wolf. *Principles of Optics*. Elsevier Ltd, 1980. ISBN: 978-0-08-026482-0.

[17] Pedrotti, F. L. *Introduction to Optic*. 2006. ISBN: 978-0131499331.

[18] Löfdahl, M. G., V. M. J. Henriques, and D. Kiselman. *A tilted interference filter in a converging beam*, Astronomy & Astrophysics **533**, A82 (2011). DOI: 10.1051/0004-6361/201117305.

[19] Dobrowolski, J. A. *Handbook of optics*. McGraw-Hill, 1995. ISBN: 0-07-047740-X.

[20] Jansa, N. "A frequency-stable diode laser system for spectroscopy and trapping of Sr atoms". Master's Thesis, Ludwigs-Maximilians-Universität München. MA thesis. 2016. URL: http://ultracold.sr/publications/thesis_nejc_jansa.pdf.

[21] Scherz, P. and S. Monk. *Practical electronics for inventors*. 3rd edition. McGraw-Hill. ISBN: 978-0-07-177133-7.

[22] *Thermistor*. Thorlabs. Hans-Böckler-Straße 6, 85221 Dachau. URL: https://www.thorlabs.com/drawings/7fb8547fbc3e9d32-6034B695-D31B-8F6F-F72529255977C9F0/TH10K-SpecSheet.pdf.

[23] Burns, G. W. and M. G. Scroger. *The calibration of thermocouple and thermocouple materials*, NIST Special Publication **250-35** (1989). URL: https://nvlpubs.nist.gov/nistpubs/Legacy/SP/nistspecialpublication250-35.pdf.

[24] Patin, N. *Power Electronics Applied to Industrial Systems and Transports*. Elsevier, 2015. ISBN: 9781785480027.

[25] Bhattacharya, P., R. Fornari, and H. Kamimura. *Comprehensive Semiconductor Science and Technology*. Elsevier Science, 2011. ISBN: 9780444531438.

[26] "The Fundamentals of Thermoelectrics". A bachelor's laboratory practical. LMU. URL: https://www.nano.physik.uni-muenchen.de/nanophotonics/_assets/pdf/f1/K3_Thermoelectrics.pdf.

[27] Moehle, K. "Piezoelectrically Tunable Optical Cavities for the Gravitational Wave Detector LISA". PhD thesis. Mathemathisch-Naturwissenschaftlichen Fakultät I, Humboldt-Universität zu Berlin, 2013.

[28] Katzir, S. and B. J. Z. *The Discovery of the Piezoelectric Effect*, Archive for History of Exact Sciences **57**, 61 (2003). DOI: 10.1007/s00407-002-0059-5.

[29] Gomez, E. S. *Piezoelectric Ceramics*. Sciyo, 2010. ISBN: 978-953-307-122-0.

[30] *SW 90 H*. Sonoswiss. Sonnenstrasse 417, 8262 Ramsen. URL: https://www.sonoswiss.ch/fileadmin/media/CleaningUnits/DataSheets/de/Datenblatt_SW_90_H.pdf.

[31] Scholl, M., W. Cairncross, and I. Kivlichan. *Interference Filter Stabilized External-Cavity Diode Lasers*, Optics Communications **266**, 609 (2012). DOI: 10.1016/j.optcom.2006.05.011.

[32] Tripathy, S. K. *Refractive indices of semiconductors from energy gaps*, Optical Materials **46**, 240 (2015). DOI: 10.1016/j.optmat.2015.04.026.

[33] *EYP-RWE-0690-00703-1000-SOT02-0000*. Eagleyard. Rudower Chaussee 29, 12489 Berlin. URL: https://www.eagleyard.com/fileadmin/downloads/data_sheets/EYP-RWE-0690-00703-1000-SOT02-0000.pdf.

[34] *20C-A4.5-02*. Schäfter+Kirchhoff. Kieler Str. 212, 22525 Hamburg. URL: https://www.sukhamburg.com/download/20C_mounting.pdf.

[35] *PS881-B-N-SF11*. Thorlabs. Hans-Böckler-Straße 6, 85221 Dachau. URL: https://www.thorlabs.de/drawings/9756d6c0f84eb368-8A6748B4-C5B2-92F9-D183047F83785292/PS881-B-AutoCADPDF.pdf.

[36] *IOT-5-670-VLP Faraday tandem isolator*. Thorlabs. Hans-Böckler-Straße 6, 85221 Dachau. URL: https://www.thorlabs.com/drawings/7fb8547fbc3e9d32-6034B695-D31B-8F6F-F72529255977C9F0/IOT-5-670-VLP-Manual.pdf.

[37] Bartl, J., R. Fira, and V. Jacko. "Thermoelectric tuning of the laser diode radiation frequency", *12th Czech-Slovak-Polish Optical Conference on Wave and Quantum Aspects of Contemporary Optics*. Vol. SPIE 4356. 2001, p. 270. DOI: 10.1117/12.417839.

[38] *Diode Laser Supply Electronics Manual*. Toptica. Lochhamer Schlag 19, 82166 Gräfelfing. URL: https://www.toptica.com/products/tunable-diode-lasers/laser-driving-electronics/sys-dc-110-analog-control/.

[39] Wiseman, H. M. *The ultimate quantum limit to the linewidth of lasers*, arXiv:quant-ph/9903082 (1999).

[40] Svelto, O. *Principles of Lasers*. 1998. ISBN: 978-1-4419-1302-9.

Acknowledgements

I am extremely thankful to Dr. Sebastian Blatt for providing me all support and guidance which made me complete the project duly.

There are a few key members whose help with building the lasers has been invaluable. I thank Dr. Neven Santić, for generous support and encouragement during the preparation this manuscript; Etienne Staub, for helping me when the technical things didn't work; Rudolf Haindl, for always going out of his way to help me with electronics; Jan Trautmann, for providing a theoretical physics support; Annie Jihyun Park, for giving much-needed direction during my thesis and André Heinz, for the best sport-diet advices.

Finally, I thank Prof. Immanuel Bloch, for giving me this excellent opportunity, to write my Bachelor thesis in the Strontium lab. Thank you.

This work was funded by the Max Planck Institute of Quantum Optics in Garching, Munich.